Journal of Marine Research, 54, 487–520, 1996

A wave-induced stirring mechanism in the mid-depth equatorial ocean

by Xianjin Li[1], Ping Chang[1] and R. C. Pacanowski[2]

ABSTRACT

A wave-induced stirring and transport mechanism for the mid-depth equatorial ocean is proposed and examined using both analytic linear equatorial wave solutions and a fully nonlinear reduced-gravity model. The study of kinematic stirring using the linear solutions suggests that a superimposition of a few simple equatorial waves can lead to strong Lagrangian stirring and transport along the equator. In particular, a combination of an annual long Rossby wave and a high-frequency Yanai wave appears to be most effective in producing strong stirring in the interior equatorial region. Further investigations of stirring properties using an inverted, fully nonlinear reduced gravity shallow-water model support the results of the kinematic stirring study. By evaluating the finite-time estimates of Lyapunov exponents, we identified two regions where chaotic stirring is most active. One is the western boundary region where short Rossby waves likely play a dominant role in producing the strong chaotic stirring. The other is the equatorial waveguide where a low-frequency Rossby wave prescribes the pattern of the stirring geometry, and a high-frequency Yanai wave plays a role of stirring the fluid. The proposed stirring mechanism provides a plausible explanation of the observed chlorofluorocarbon distribution found in the mid-depth equatorial Atlantic Ocean.

1. Introduction

It is well-known that the southward spreading of cold and saline North Atlantic Deep Water (NADW), formed in the Labrador Sea and north of Iceland region, continues to cross the equator along the South American continental slope as a deep western boundary current (DWBC). However, studies of the distribution of water-mass properties such as salinity, oxygen, and nutrients (Wust, 1935; Reid, 1982; Kawase and Sarmiento, 1986) or anthropogenic tracers like chlorofluorocarbons (CFCs) (Weiss *et al.,* 1985, 1990) show an eastward spreading of NADW tracers along the equator, suggesting that only part of the upper NADW penetrates into the Southern Hemisphere. In a recent analysis, Weiss *et al.* (personal communication) noticed that a wedge of CFCs initially observed in 1982–83 in the western equatorial

1. Department of Oceanography, Texas A & M University, College Station, Texas, 77843-3148, U.S.A.
2. Geophysical Fluid Dynamics Laboratory/NOAA, Princeton University, Princeton, New Jersey, 08542, U.S.A.

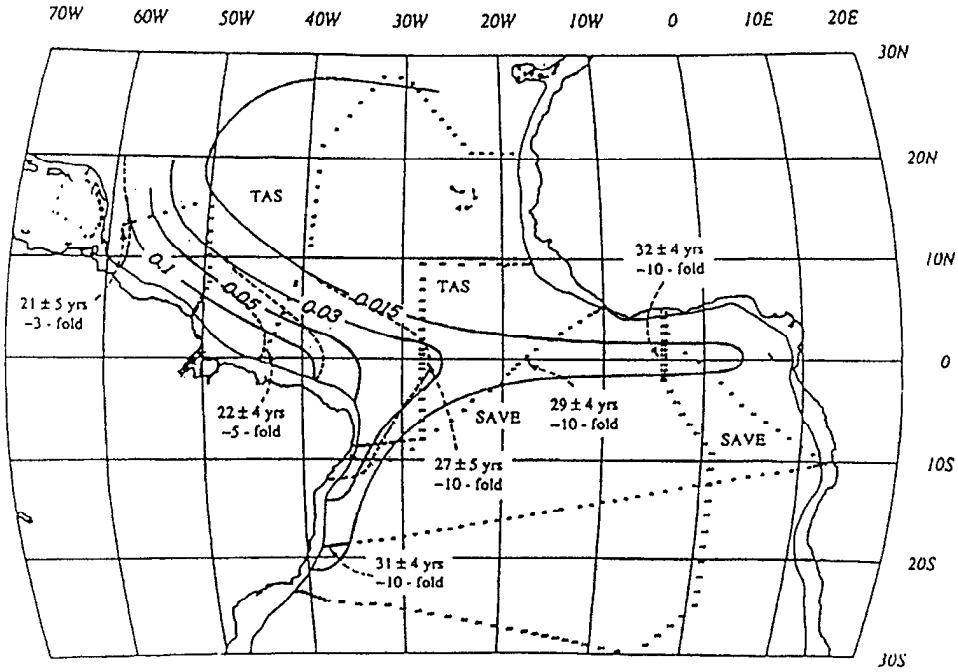

Figure 1. Distribution in 1982–83 (dashed line) and 1987–88 (solid line) of F-11 concentration in pmol/kg on the $\sigma_{1.5}$ = 34.63 kg m^{-3} density surface which marks the Upper North Atlantic Deep Water (UNADW) CFM feature (1982–83 from Weiss *et al.*, 1985; 1987–88, Courtesy of R. Weiss, unpublished work). The depth of this density surface in the equatorial Atlantic is about 1.7 km.

Atlantic at depth of about 1700 m (Weiss *et al.*, 1985) developed into a strikingly long but narrow equatorial tongue during a five-year period (Fig. 1). This rapid spreading of tracers along the equator in the mid-depth equatorial Atlantic Ocean implies an important transport process which is currently poorly understood. This study attempts to improve our understanding of stirring and transport process in the mid-depth equatorial oceans. We propose that equatorially-trapped waves play an important role in stirring and transporting water particles along the equator and that wave-induced stirring and transport are responsible for the rapid formation of the narrow equatorial tracer tongue noted above.

Existing observations in the deep equatorial Atlantic Ocean indicate that flows between 1000 m and 3000 m in depth are highly time-dependent. Current meter measurements in both the eastern (Weisberg *et al.*, 1979, Weisberg and Horigan, 1981) and western (Ponte *et al.*, 1990) Atlantic Ocean showed that the zonal velocities of the equatorial currents at these depths vary on a seasonal-to-interannual time scale, with peak-to-peak changes approaching 20 cm s^{-1}. The variability of these

currents is much larger than the time-mean values. The low-frequency (annual or interannual) variability of the deep equatorial currents arguably derives its energy from surface wind forcing through the vertical propagation of low-frequency Rossby waves (Lukas and Firing, 1985; Kessler and McCreary, 1993). Superimposed on this low-frequency variability is a high-frequency signal with a period ranging from 30–60 days which dominates fluctuations in the meridional component of the currents. Weisberg *et al.* (1979), Weisberg and Horigan (1981) and Ponte *et al.* (1990) reported 10–15 cm s^{-1} fluctuations of meridional velocity on the equator in the 1000–3000 m depth range. Highly transient currents in the mid-depth of the Atlantic Ocean are reinforced by the more recent study of Richardson and Schmitz (1993) where both low- and high-frequency oscillations are observed along individual SOFAR float paths. In particular, the float trajectories within the interior equatorial region exhibit high-frequency (about 30 to 60 days) oscillations in the meridional direction, apparently associated with equatorially-trapped Yanai (also referred to as mixed Rossby-gravity) waves.

A recent numerical modeling study of Böning (1993) using a high-resolution Ocean General Circulation Model (OGCM) of the Atlantic basin revealed deep circulation features that are qualitatively similar to the observations. He found that the modeled deep equatorial circulation is dominated by alternating eastward and westward currents in the equatorial belt between 5S and 5N, which was attributed as long equatorial annual Rossby waves forced by the seasonally-varying winds. Core speeds of the oscillating current exceed 15 cm s^{-1}. The time-mean equatorial zonal currents around 1800 m are less than 1 cm s^{-1} despite a well-developed salinity tongue of NADW extending eastward along the equator at this depth range. In addition to the low-frequency variability, a distinct high-frequency Yanai wave was also found in mid-depth of the model ocean. Based on the theoretical studies of Philander (1978) and the numerical analysis of Cox (1990), Böning speculated that near-surface instability waves generated by the strong shear between the South Equatorial Current (SEC) and the North Equatorial Countercurrent (NECC) in the upper oceans may provide the energy source for the deep Yanai wave. A synthesis of these observational and numerical results indicates that the deep equatorial circulations are strongly influenced by wave activities. It is of interest to explore how these waves can contribute to the stirring and transport of water particles in the deep equatorial oceans.

In the oceans, heat, salt, and tracer elements are transported from place to place by the Lagrangian displacement of water particles. In certain regions of the oceans, such as the mid-depth equatorial Atlantic where velocity fluctuations are considerably larger than the Eulerian mean velocity, the velocity of the water particles advected by the Lagrangian mean velocity may not agree with the Eulerian velocity (see for example, Longuet-Higgins, 1969). Recent studies of chaotic stirring of fluids

suggest that relatively simple periodic wave motions can give rise to spatially-complicated particle behavior (see Aref, 1984; Ottino *et al.,* 1988, for a review). These theoretical studies identified a stirring process called chaotic stirring, in which Lagrangian dispersion is a result of simple wave motion even without random components in the underlying velocity field. The concept of chaotic stirring has recently been applied to understand stirring processes in idealized geophysical fluid systems (Weiss, 1991; Pierrehumbert, 1991a, b; 1993); in the middle atmosphere (Bowman, 1993a,b) and in the coastal oceans (Ridderinkhof and Zimmerman 1992). Since the deep equatorial circulation in the Atlantic Ocean is dominated by wave-like motions, it is reasonable to speculate that Lagrangian advection and dispersion induced by wave motions may have strong influences on stirring and transport of water particles along the equator. However, the concept of chaotic stirring and transport is based on wave kinematics without taking into consideration the nonlinear dynamical effect. In reality, dynamical effects can also contribute significantly to stirring and transport processes in the oceans. Therefore, when chaotic stirring is applied to the study of deep equatorial circulation, one must consider effects of both wave kinematics and wave dynamics. Stirring and transport in the real equatorial ocean may be found between the extremes of Lagrangian chaos and classical diffusion.

The effect of wave motions forced by upper ocean variability on the deep equatorial circulation was examined by Thompson and Kawase (1993). Using a one and a half layer, inverted reduced-gravity model forced by a wave maker near the eastern boundary, they showed that the equatorially-trapped long Rossby wave can set up a recirculation gyre in the western boundary region where significant stirring of fluid parcels occurs. In the interior, strong stirring of fluid parcels was not found and fluid parcels simply travel westward due to Stokes' drift.

Our study focuses on stirring process in the interior of the equatorial region. In particular, we investigate the Lagrangian stirring and transport processes in the deep equatorial Atlantic in the context of an inverted, reduced-gravity model. We shall show that a strong stirring can exist in the interior equatorial region if the flow field contains more than one wave. In Section 2, we first study the Euler-Lagrangian transformation and the Stokes' drift given by equatorial-trapped waves, then wave-induced chaotic stirring is investigated with linear, equatorially-trapped wave solutions. Lagrangian disperson is examined by simulating a large number of Lagrangian particles. In Section 3, we discuss the results from particle simulations in both linear and nonlinear reduced-gravity models with emphasis on the temporal and spatial evolution of finite-time Lyapunov exponents. Finally, in Section 4 we summarize the major findings and discuss implications of these findings to the observed tracer distribution in the deep Atlantic Ocean.

2. Stirring and transport induced by linear equatorial waves

Given an Eulerian velocity field, Lagrangian particle locations $x(t)$ and $y(t)$ are determined by solving a system of coupled ordinary differential equations:

$$\frac{dx}{dt} = u(x, y, t) \tag{1}$$

$$\frac{dy}{dt} = v(x, y, t) \tag{2}$$

subject to initial conditions $[x(0), y(0)] = (x_0, y_0)$. These define a kinematic relation between the Eulerian velocity field and the Lagrangian particle location which is often referred to as Euler-Lagrangian transformation. Such a transformation is nonlinear even when the Eulerian velocity is composed of simple, linear wave motions. Because of this nonlinèarity, a simple deterministic velocity field can produce efficient stirring and transport. In the simplest case, where the flow field is governed by a small-amplitude single-frequency 1-D traveling wave, the nonlinearity in the Euler-Lagrangian transformation produces a Stokes' drift: particles drift in the direction (or opposite direction) of the wave propagation with a drift speed proportional to the square of the wave amplitude. As the wave amplitude increases, particle trapping can occur, in which particles are carried with the wave at the wave's phase speed in certain regions of the fluid. When the flow field contains more than one wave, the possibility of chaotic particle trajectories arises, where simple velocities can produce efficient particle displacements in such a way that the combined action of stretching and folding produces exponential growth of the distance between two particles which originally were close together. This so-called Lagrangian chaotic stirring and transport refers to the fact that the trajectory of a particle advected by a deterministic velocity field can nevertheless be chaotic. The concept of chaotic stirring differs considerably from the classical concept of shear dispersion in which a turbulent velocity field needs to be present for an effective dispersion of water particles.

To illustrate these theoretical concepts, we consider Lagrangian particle motions in the presence of either a single equatorial wave or a superimposition of two equatorial waves. In particular, we focus on two special equatorial waves—an annual long Rossby wave and an intraseasonal Yanai wave, because these waves appear to dominate the interior flow of the mid-depth equatorial Atlantic Ocean.

We start our analysis by assuming a two-dimensional time-dependent velocity field $[u(x, y, t), v(x, y, t)]$ is given by

$$u = A_1 u_1 + A_2 u_2 \tag{3}$$

$$v = A_1 v_1 + A_2 v_2 \tag{4}$$

where u_i and $v_i (i = 1, 2)$ are the zonal and meridional velocity components of two equatorially-trapped waves. In our case, u_1 and v_1 are chosen to be the first-meridional-mode ($n = 1$) of a long Rossby wave of annual period, and u_2 and v_2 to be a Yanai wave of period of 45 days. According to equatorial wave theory (Moore and Philander, 1977), u_1 and v_1 can be written as

$$u_1 = (q - r) \sin (k_1 x - \omega_1 t + \phi_1)/2 \tag{5}$$

$$v_1 = D_1((2\beta/c)^{1/2} y) \cos (k_1 x - \omega_1 t + \phi_1) \tag{6}$$

and u_2 and v_2 can be written as

$$u_2 = -(\omega_2 y/c) \exp (-\beta y^2/2c) \sin (k_2 x - \omega_2 t + \phi_2) \tag{7}$$

$$v_2 = \exp (-\beta y^2/2c) \cos (k_2 x - \omega_2 t + \phi_2) \tag{8}$$

where

$$q = (ck_1 - \omega_1)^{-1} (2\beta c)^{1/2} D_2((2\beta/c)^{1/2} y) \tag{9}$$

$$r = (ck_1 + \omega_1)^{-1} (2\beta c)^{1/2} D_0((2\beta/c)^{1/2} y) \tag{10}$$

$D_i(y')$ $(i = 0, 1, 2)$ are parabolic cylinder functions and ϕ_i $(i = 1, 2)$ are phase lags. The zonal wavenumber of the Rossby wave k_1 and the Yanai wave k_2 correspond to frequencies ω_1 and ω_2 according to the dispersion relations

$$\omega_1 = -\beta k_1/((k_1)^2 + (2n + 1)\beta/c) \tag{11}$$

and

$$k_2 = \omega_2/c - \beta/\omega_2 \tag{12}$$

respectively. In our calculation, we chose $n = 1$ (first mode), $\omega_1 = 2\pi/1$ year and $\omega_2 = 2\pi/45$ days. The other parameters are set as follows: the characteristic speed $c = 100$ cm s^{-1}, $\beta = 2.3 \times 10^{-13}$ cm^{-1} s^{-1}, $\phi_1 = 0$ and $\phi_2 = 0$ (these phase-lags of ϕ_i are used throughout this study, unless otherwise noted). Wave amplitude coefficients A_1 and A_2 are varied to examine effects of waves on stirring and transport of water particles.

Once the time-dependent velocity field is given, particle trajectories are obtained by solving Eq. (1) and (2) numerically using a fourth-order Runge-Kutta method. Since we are interested in particle dispersion which requires a large ensemble of trajectories, we use 10,000 particles in a typical calculation. In most of the calculations presented, we use a periodic channel which allows particles to re-enter the domain from the one end after leaking out from the other.

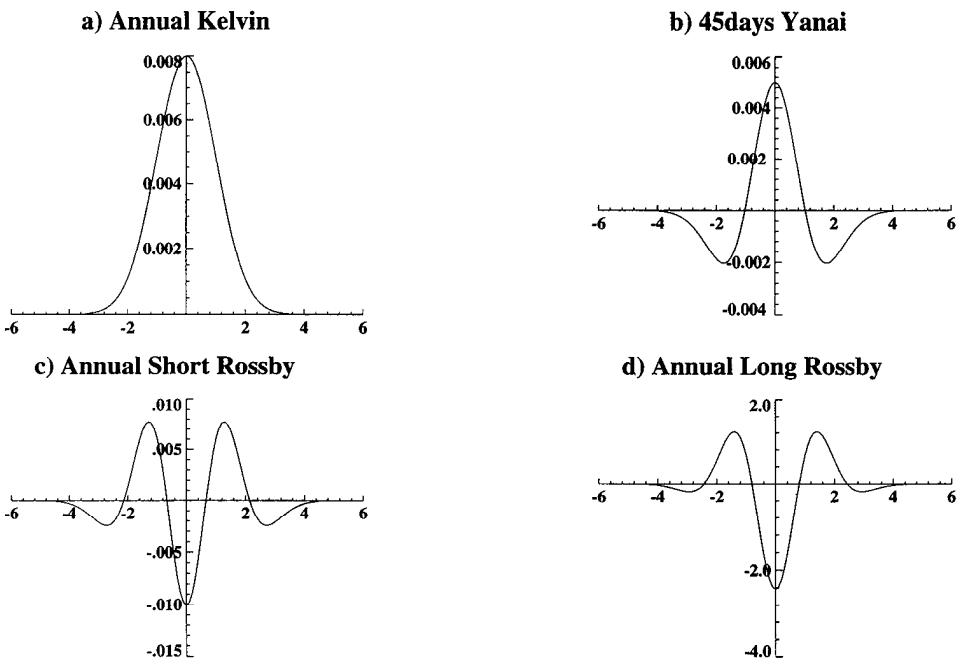

Figure 2. Meridional profiles of the Stokes' drift (unit: cm s^{-1}) induced by an annual Kelvin wave (a); a 45-day period Yanai wave (b); an annual short Rossby wave ($n = 1$) (c); an annual long Rossby wave ($n = 1$) (d). Note that the vertical scale in (d) is much larger than that in the other three cases. The characteristic speed of the model ocean ($C = 100$ cm s^{-1}). The corresponding analytical solutions are shown in the Appendix.

a. Stokes' Drift. Single-frequency traveling waves with infinitesimal amplitude transport energy and momentum but not particles (or mass). As the wave amplitude increases, spatial variations of the total Eulerian velocity can produce a Stokes' drift. Analytic solutions for the Stokes' drift induced by various equatorial waves can easily be derived. The solution procedure can be found in Longuet-Higgins (1969, 1972) and Zimmerman (1979, 1986). A brief outline of the equatorial Stokes' drift is given in the Appendix. Figure 2 shows examples of meridional profiles of Stokes' drift induced by an annual Kelvin wave, annual Rossby waves and a high-frequency Yanai wave, respectively. Symmetric ($n = 1, 3, \cdots$) Rossby waves produce a westward (negative) Stokes' drift near the equator and an eastward (positive) drift off the equator, while the Yanai wave produces a Stokes' drift in the opposite sense. In general, the Stokes drift is strongest on the equator. For the same wave amplitude, the Stokes' drift induced by an annual long Rossby wave (~ 2.0 cm s^{-1}) is much larger than that of an annual Kelvin (~ 0.008 cm s^{-1}) or Yanai wave (~ 0.005 cm s^{-1}).

Figure 3a shows a map which is constructed by superimposing "snapshots" of the 10,000 particle locations at $t = 1, 2, 3 \cdots$ years in the presence of a single annual long Rossby wave with amplitude $A_1 = 2.0$ cm s^{-1}. (This mapping technique is similar to

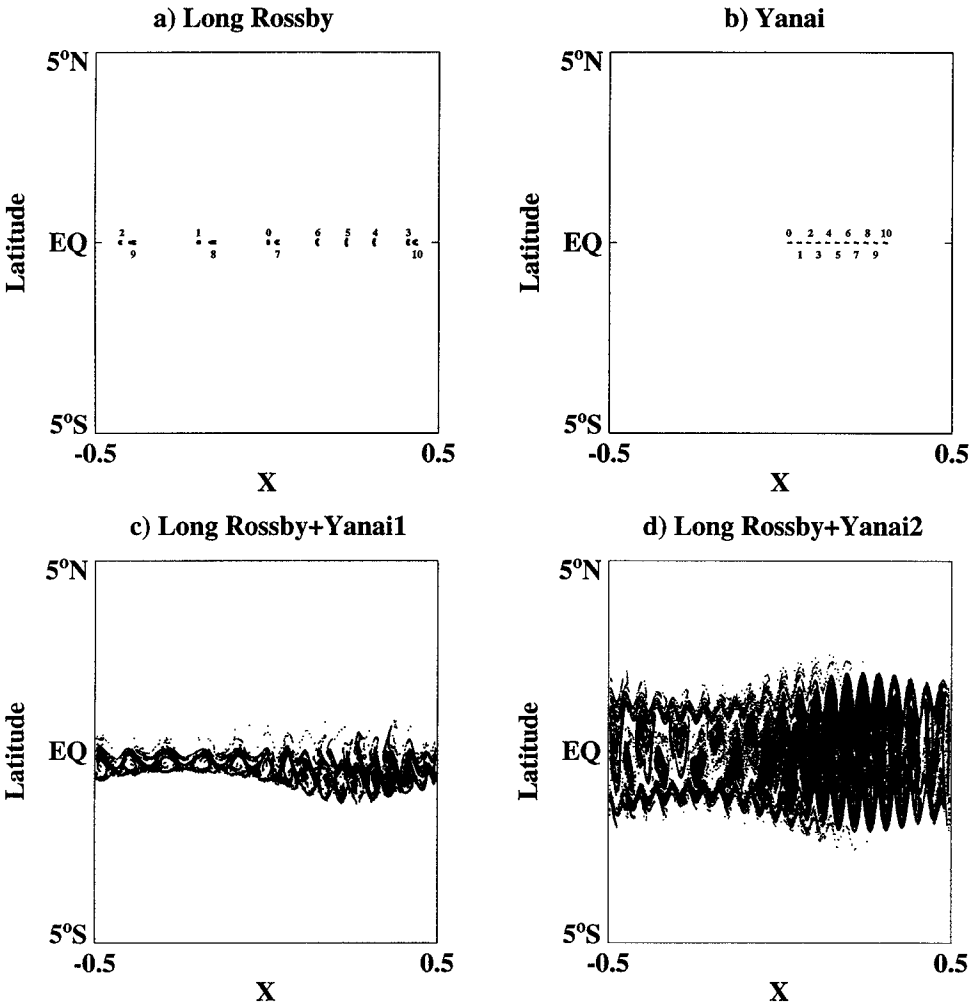

Figure 3. Mapping of 10,000 particles for (a) a single annual long Rossby wave (A_1 = 2.0 cm s^{-1}, ϕ_1 = 0); (b) a single Yanai wave (A_2 = 10 cm s^{-1}, ϕ_2 = 0); (c) both waves (A_1 = 2.0 cm s^{-1}, ϕ_1 = 0 and A_2 = 1 cm s^{-1}, ϕ_2 = 0); (d) same as (c) except A_2 = 10 cm s^{-1}. The iteration number of "snapshot" (marked beside the particles) in (a) and (b) is N = 10; in (c) and (d) N = 20. The numbers around the patch of particles in (a) and (b) are the time of "snapshot." The X coordinate is nondimensionalized by the wavelength of annual long Rossby wave ($\lambda \approx 94°$) in (a), (c), (d) or the wavelength of Yanai wave ($\lambda \approx 4.47°$) in (b).

Poincaré mapping except it uses many particles with a few iterations.) The particles are initially located around the origin x = 0 and y = 0. The 10,000 particles drift westward along the equator with little zonal spreading even after 10 years. The westward drifting is due to Stokes' drift. A similar mapping is shown in Figure 3b for a single Yanai wave case. The interval of "snapshot" here is 45 days (the period of

the Yanai wave). Note that the zonal displacement is much smaller than that of the annual Rossby wave and that the Stokes' drift is eastward. Chaotic stirring is not evident here either. The result that chaotic stirring is absent when the governing two-dimensional flow field contains only a single wave is consistent with the general theory of chaotic stirring. This is because, in the co-moving reference frame $x' = x - c_1 t$ ($c_1 = \omega_1/k_1$), the Eulerian velocity of a single wave describes a steady flow which has two degrees of freedom. It is well-known that chaotic motion cannot occur in a dynamical system with less than three degrees of freedom. It also should be kept in mind that the Euler-Lagrangian transformation (1) and (2) is a purely kinematical way of stating that the Lagrangian velocity can be derived from the prescribed Eulerian velocity field without requiring any further dynamics. Moore (1970) pointed out that, when the second-order dynamic effects (terms like $\overline{u'v'}$, $\cdots$, etc.) are included, the Stokes' drift is usually weakened. This result will be confirmed by our numerical simulations in Section 3. In particular, the mean Eulerian velocity produced by the second-order dynamic effects will completely cancel the Stokes' drift in a closed basin containing no closed geostrophic contours without dissipative processes. However, Moore did not take chaotic stirring into account when there is more than one wave in the flow field.

b. Chaotic mixing. When a second wave of different frequency is introduced, the possibility of chaotic particle trajectories arises because the number of degrees of freedom in the dynamic system is no longer less than three. Figure 3c depicts a similar map to Figure 3a for the case when a small-amplitude Yanai wave ($A_2 = 1.0$ cm s^{-1}) is superimposed on the annual Rossby wave in Figure 3a. In contrast to Figure 3a, strong particle dispersion is clearly observed. To further illustrate the dispersion, in Figure 4 we display the time evolution of the position of 10,000 particles placed within a small disk centered at the origin $x = 0, y = 0$ at $t = 0$. In the initial stage, the small disk quickly stretches into a short segment, which then moves around in the fluid for several periods without further deformation. The behavior at this stage is called sticking (See for example, Solomon *et al.,* 1994; Weeks *et al.,* 1994). Then a period of rapid elongation of the segment occurs. This eventually leads to break-up of the segment. After this occurs, particle motion appears to be chaotic in a rope-shaped region about the equator. It is within this region that chaotic stirring is most active. This region broadens meridionally when the amplitude of Yanai wave A_2 is increased to 10 cm s^{-1} (Fig. 3d).

The dispersion of a group of particles can also be described by the displacement covariance

$$\sigma^2(t) = \langle (x(t) - \langle x(t) \rangle)^2 \rangle \tag{13}$$

where $\langle\ \rangle$ is the average over an ensemble of many tracer particles. The covariances $\sigma^2(t)$ for the four cases considered in Figure 3 are shown in Figure 5. There is almost

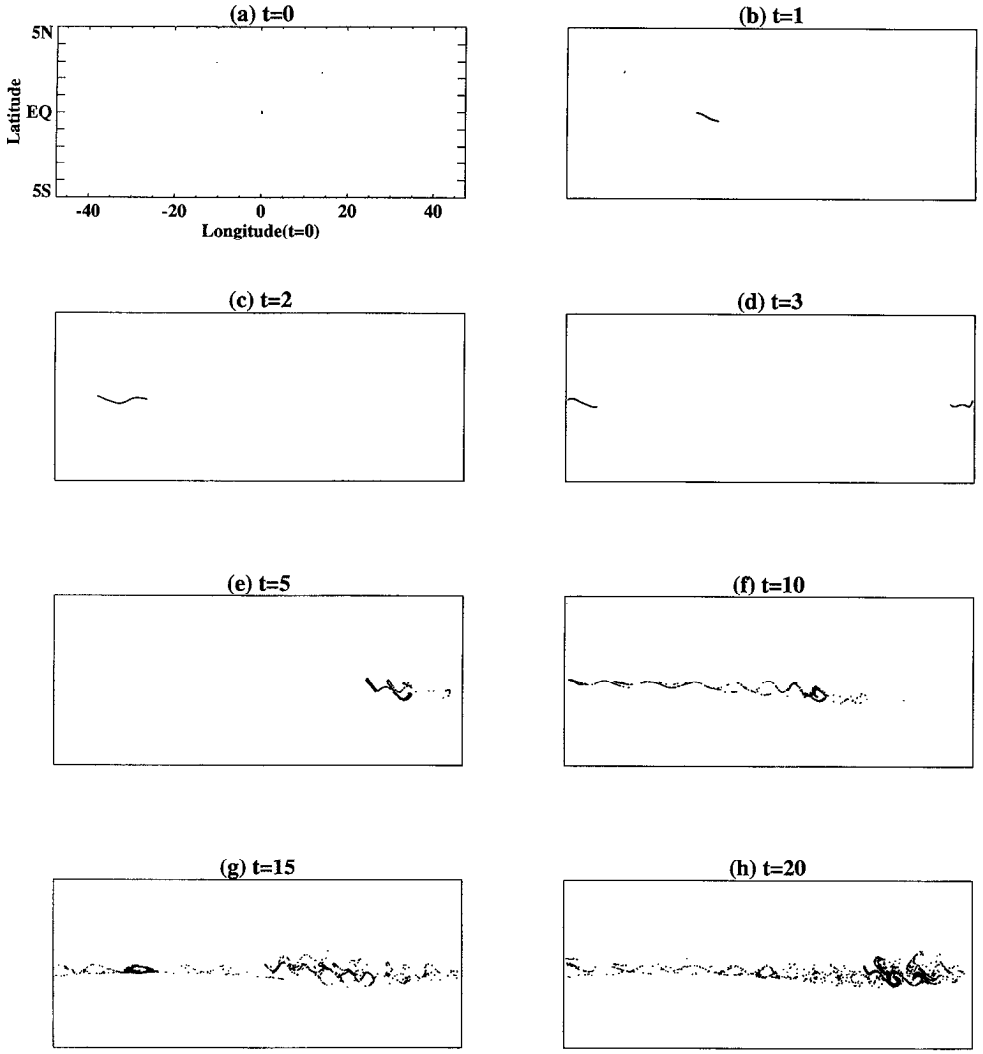

Figure 4. Time courses of trajectories of an ensemble of 10,000 particles which are originally located around (0.0, 0.0) in a channel where there is an annual long Rossby wave (A_1 = 2.0 cm s^{-1}, ϕ_1 = 0) and T = 45 days Yanai wave (A_2 = 1 cm s^{-1}, ϕ_2 = 0) at t = (a) 0; (b) 1; (c) 2; (d) 3; (e) 5; (f) 10; (g) 15; (h) 20 years.

no dispersion in the case of only a single annual long Rossby wave or a single Yanai wave ($\sigma^2(t) < 0.1$ for single Rossby wave and 2.0×10^{-4} for single Yanai wave). However, in the cases where both a high-frequency Yanai wave and an annual Rossby wave are present, the displacement covariances grow exponentially after several periods of sticking. Their magnitude is several orders larger than that in the single-wave case, indicating the presence of strong particle dispersion and stirring.

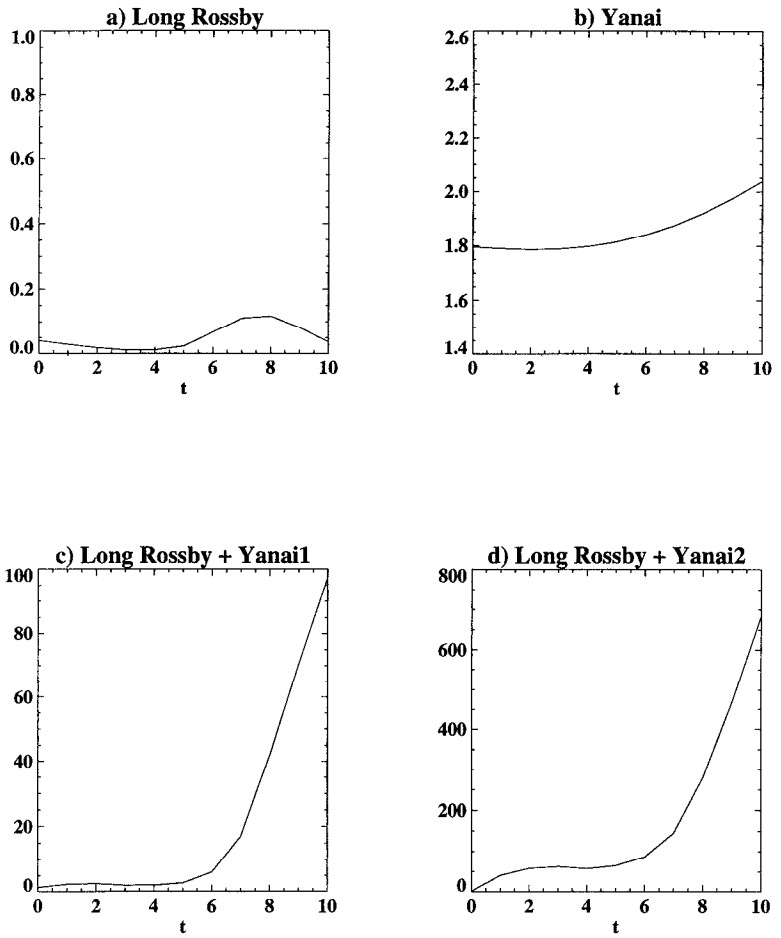

Figure 5. Covariance of the zonal location (x in *degree*) of the group of particles $\sigma^2(t)$ as a function of time t (year) for the four cases in Figure 3 ($\sigma^2(t) \sim t$). In order to calculate the covariance, we removed the periodic channel boundary condition, so the particles go freely according to relations (1) and (2). In particular, the unit in (b) is 10^{-4}*degree*^{2} while in the other three panels it is *degree*^{2}.

There is a transient period between the initial sticking period and the later strong dispersion period. The evolution of such transition is shown in Figure 6, where 2,500 particles are initially released within a square box 1° × 1° ($A_1 = 2.0\,\text{cm s}^{-1}$, $A_2 = 10.0\,\text{cm s}^{-1}$ and $\phi_1 = \pi$, $\sigma_2 = 0$). The interval of every "snapshot" is 45 days. Note that there is no periodic channel boundary condition used here. Sticking and strong dispersion are clearly displayed.

Chaotic stirring takes the form of "anomalous" diffusion which differs considerably from turbulent diffusion (Solomon *et al.,* 1994). To quantify this difference, we

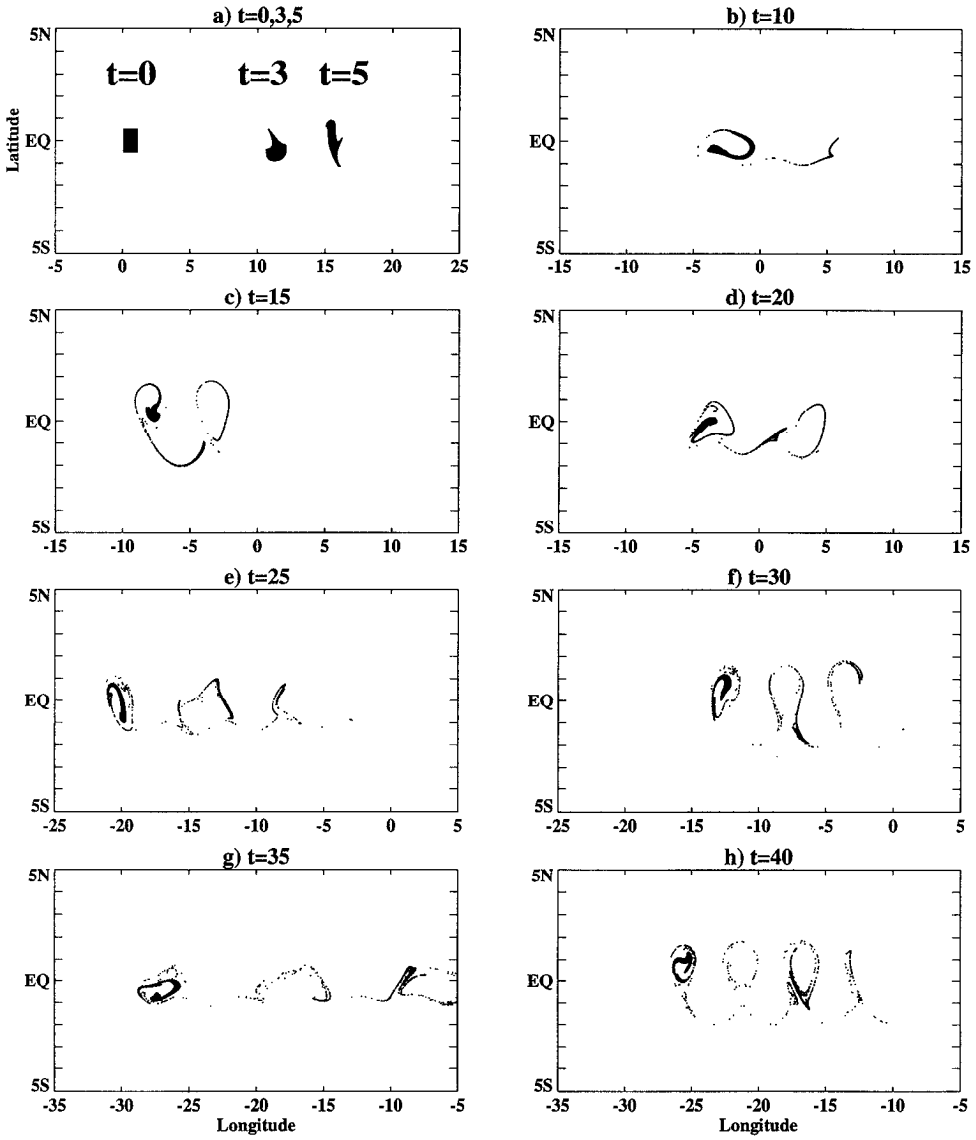

Figure 6. Time courses of trajectories of an ensemble of 2,500 particles which are originally located around (0.0, 0.0) in a channel where there is an annual long Rossby wave (A_1 = 2.0 cm s^{-1}, $\phi_1 = \pi$) and T = 45 days Yanai wave (A_2 = 10 cm s^{-1}, $\phi_2 = 0$) at t = (a)0, 3, 5; (b) 10; (c) 15; (d) 20; (e) 25; (f) 30; (g) 35; (h) 40 time units (Here 1 unit = 45 days). Note the different zonal range in different plot.

compute the displacement covariance $\sigma^2(t)$ for the experiment shown in Figure 6. In general, $\sigma^2(t)$ grows as t^ν where ν depends on flow field properties. In a 2-D turbulent flow where diffusion is produced by purely random motion, ν is equal to one and the stirring is "normally diffusive." The stirring is considered "superdiffusive" for $\nu > 1$

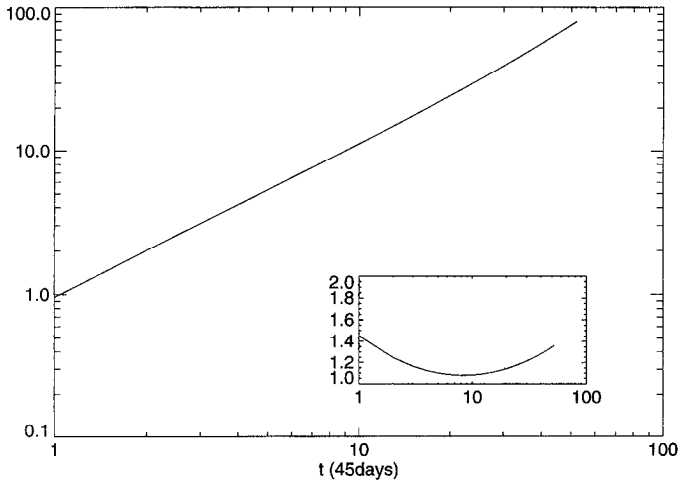

Figure 7. Log-log plot of the covariance of zonal location (x) of the group of particles $\sigma^2(t)$ as a function of time t for the case in Figure 6. The inner panel is a linear-log plot of the coefficient of ν as a function of time ($\nu \sim \log t$).

and "subdiffusive" for $\nu < 1$ (Weeks *et al.* 1994). In the case we considered here, ν is between 1.10 and 1.45 (Fig. 7), suggesting that superdiffusion is in action.

To summarize the stirring and transport processes induced by the superposition of an annual long Rossby wave and a 45-day Yanai wave, Figure 8 displays a series of snapshots of a patch of 10,000 particles distributed in a 4° × 4° square box (0.0° − 4.0°; 2.0S−2.0N) (Fig. 8a) where $A_1 = 2.0$ cm s^{-1}, $A_2 = 5.0$ cm s^{-1}, $\phi_1 = 0$ and $\phi_2 = 0$. As time progresses, particles off the equator begin to drift eastward while particles near the equator spread westward (Fig. 8b-c). The zonal spreading of particles along the equatorial waveguide is primarily due to the Stokes' drift of the annual long Rossby wave. After initial spreading, particle filaments are generated near the equator through stretching and folding, indicating that chaotic stirring induced by the joint effects of the long annual Rossby and high-frequency Yanai waves becomes active (Fig. 8d–g). Chaotic stirring intensifies and particle distribution becomes more and more homogeneous in the narrow equatorial band as the integration continues. After 20 years, the partcicles are spread more or less uniformly along the equator although we can still distinguish the sticking segment (Fig. 8h). Throughout the process, the long Rossby wave seems to play the role of prescribing the envelope of the stirring geometry and the high-frequency Yanai wave the role of stirring fluid within the narrow equatorial band. A complete determination of stirring geometry in the given wave field is difficult because both the long Rossby and Yanai waves are divergent flows. Therefore, the Eulerian velocity cannot be simply described by a stream function and the governing dynamical system is nonHamiltonian. In previous studies by Weiss (1991) and Pierrehumbert (1991a), where chaotic stirring is considered in a framework of a 2-D nondivergent barotropic

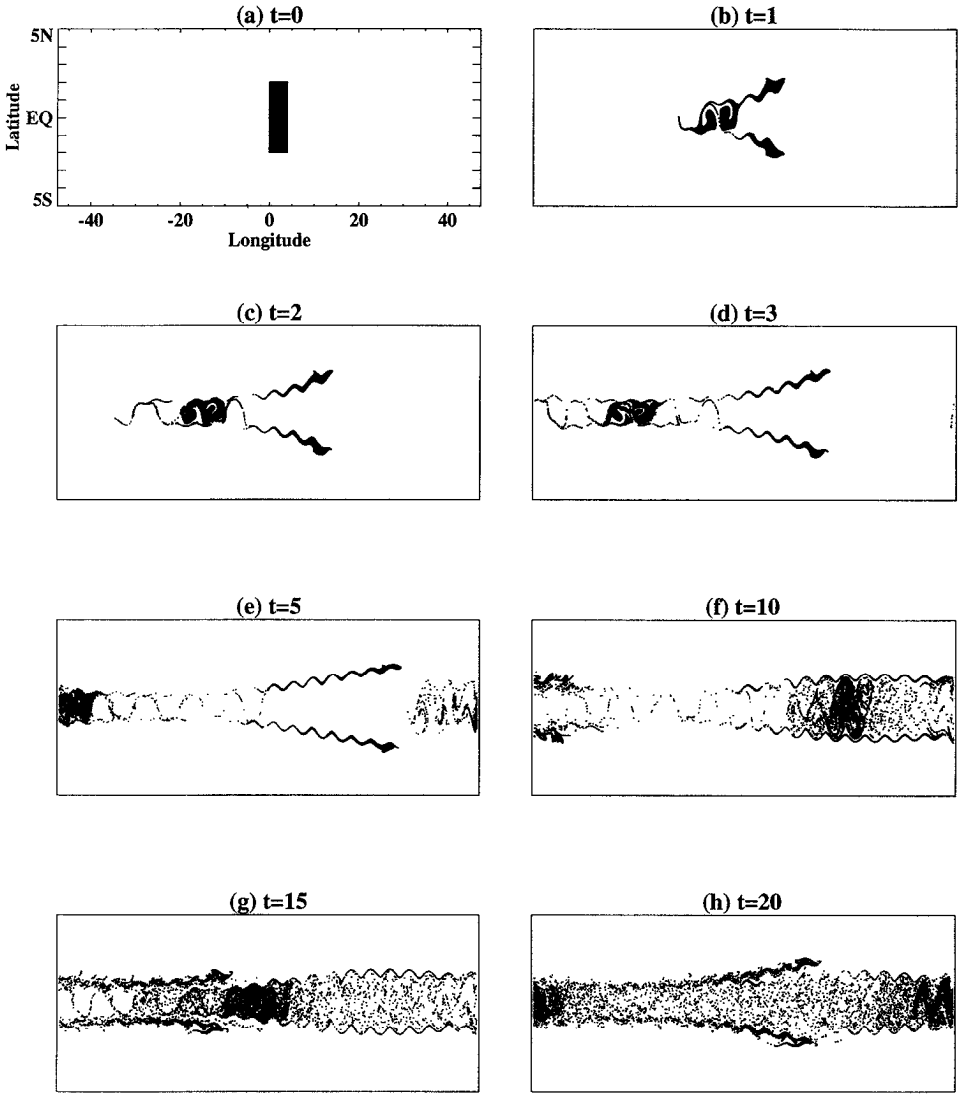

Figure 8. Time courses of trajectories of a patch of 10,000 particles which are originally located within a box 5° × 4° around (2.5, 0.0) in a channel where there is an annual long Rossby wave (A_1 = 2.0 cm s^{-1}, ϕ_1 = 0) and T = 45 days Yanai wave (A_2 = 5 cm s^{-1}, ϕ_2 = 0) at t = (a) 0; (b) 1; (c) 2; (d) 3; (e) 5; (f) 10; (g) 15; (h) 20 years.

Rossby wave, the stirring geometry and efficiency can be obtained by analyzing the wave stream function to determine a special trajectory called the separatrix, which separates the particle-trapping region from the free region. It is shown that a chaotic stirring region is a result of the breakup of the separatrix. This region is often bounded by Kolmogorov-Arnold-Moser (KAM) curves and particles in such a region

chaotically alternate between being trapped and carried with the wave, and being free and drifting backward relative to the wave, resulting in chaotic stirring. This concept of chaotic stirring may still be applied to explain the stirring in our problem. However, the analytical tools developed in the study of Hamiltonian chaos cannot be applied to determine the stirring geometry.

Although in this section we have given a detailed description of chaotic stirring induced by a superposition of a long annual Rossby wave and a high-frequency Yanai wave, the role other equatorially-trapped waves play in producing chaotic stirring has also been examined. We have found that a superposition of a short and a long annual Rossby wave also generates very strong stirring. In reality, short annual Rossby waves are most active near the western boundary region because of their small group velocities. Therefore, one anticipates that these waves play an active stirring role near the western boundary region but not in the interior equatorial region. A combination of a long annual Rossby wave and a high-frequency Kelvin wave is less effective in stirring, presumably because the Kelvin wave has none of the crucial meridional velocity component which seems necessary to produce strong stirring. In summary, the study of the kinematics of stirring in the presence of linear equatorial waves suggests that an annual Rossby wave combined with a high-frequency Yanai wave may be crucially important for stirring water particles along the equator in the interior of the mid-depth Atlantic Ocean. However, we caution that the results obtained so far are based entirely upon the kinematic relation (1) and (2) with no consideration of dynamical effects. To include nonlinear dynamical effects, in the following section we use a high-resolution, fully-nonlinear, inverted, reduced-gravity model to further explore wave-induced stirring and transport processes in the deep equatorial ocean.

3. Numerical model simulation

a. Model description. Taking the viewpoint that equatorial wave dynamics and the associated stirring and transport can be profitably studied with models complicated enough to include nonlinearity but economic enough to permit simulations of a large number of Lagrangian particles, an inverted 1½ layer reduced-gravity model is adopted to approximate an active abyssal layer of water under a stagnant upper layer. This type of model, because of its simplicity, has been often used to gain theoretical understanding of fundamental physics of abyssal circulation. For example, Kawase (1987) applied such a model to the study of the establishment of Stommel-Aron circulation (1960). Thompson and Kawase (1993) used a similar model to examine effects of nonlinear wave dynamics of deep equatorial circulation. Since the 1½ layer reduced-gravity model contains all the elements of nonlinear equatorial waves and is computationly efficient, it is ideal for the further testing of the proposed wave-induced stirring mechanism. In this study, a flat-bottom, rectangular basin of 30° × 30° centered on the equator is chosen to approximate the deep

Table 1. Parameters used in the model.

equivalent depth	H_0	10 cm
characteristic speed	$c = \sqrt{gH_0}$	$\approx$ 100 cm s^{-1}
Laplacian friction	$\mu = \kappa$	1.25×10^6 cm^2 s^{-1}
Newtonian damping	γ	$\left(\exp\left[-\left(\frac{y - 15^\circ}{2.5^\circ}\right)^2\right] + \exp\left[-\left(\frac{y + 15^\circ}{2.5^\circ}\right)^2\right]\right)/D_0$
Rayleigh friction	α	$\alpha = \gamma$
damping time scale	D_0	0.5 day
zonal resolution	Δx	0.2°
meridional resolution	Δy	0.1°

equatorial Atlantic. The effects of bottom topography and irregular coastal boundaries are not included. These effects will be examined in subsequent studies. The governing equations of motion in this idealized ocean are given by

$$\frac{Du}{Dt} - f(y)v = -g\frac{\partial \eta}{\partial x} - \gamma u + \mu\nabla^2 u \tag{14}$$

$$\frac{Dv}{Dt} - f(y)u = -g\frac{\partial \eta}{\partial y} - \gamma v + \mu\nabla^2 v \tag{15}$$

$$\frac{\partial \eta}{\partial t} + \frac{\partial[(H + \eta)u]}{\partial x} + \frac{\partial[(H + \eta)v]}{\partial y} = -\alpha\eta + \kappa\nabla^2\eta + Q \tag{16}$$

with

$$\frac{D}{Dt} = \frac{\partial}{\partial t} + u\frac{\partial}{\partial x} + v\frac{\partial}{\partial y} \tag{17}$$

where x and y are the longitude and latitude; u and v the eastward and northward velocities; Q forcing on the continuity equation; η the perturbation of the layer thickness and H the mean depth of the model ocean (which could include the bottom topography). A linear version of this reduced-gravity ocean model will be used in conjunction with the full model to study the nonlinear dynamic effects. Using the linear model permits direct comparison with results from the analytical solutions in Section 2 derived from linear equations, so that the validity of kinematical stirring theory can be examined.

The model is formulated using the enstrophy-conserving scheme of Sadourney (1975) based on the Arakawa-C grid on a spherical coordinate (Arakawa and Lamb, 1981). All parameters used in the model are listed in Table 1. A similar model was employed by Thompson and Kawase (1993) to study the role of long Rossby wave in setting up deep equatorial circulations. Several fluid particles are traced in their model simulation to understand the effect of Stokes' drift in the interior equatorial region. Since our focus is on wave-induced stirring and transport, a large ensemble of

particles is employed in our simulations. To accurately track particles in the model, trajectories of free-flowing particles are computed using a fourth-order Runge-Kutta scheme. At each time-step, horizontal interpolation is made using the neighboring 16 grid points to obtain the fluid velocity at the particle position. A bicubic interpolation using a four-by-four square of grid points surrounding the particle is employed to reduce truncation errors introduced by numerical discretization. Once particle locations are determined at each time-step, a deformation matrix of the velocity field at those locations is computed and used to evaluate the spatial distribution of finite-time Lyapunov exponents. The detailed procedure for computing Lyapunov exponents can be found in the Appendix. Finite-time estimates of Lyapunov exponents provide a good measure of the strength of chaotic stirring. This powerful technique has recently been applied to identify the strong stirring zone and barrier in the polar vortex of the upper atmosphere (Pierrehumbert, 1993; Bowman, 1993a, b). To obtain an accurate estimate of Lyapunov exponents distribution, large numbers of particles are required. In a typical simulation described below, 40,000 Lagrangian particles are used. Since our main interest is an understanding of stirring and transport in the western and central equatorial region, we seed the particles in an $8° \times 20°$ area located symmetrically about the equator near the western boundary in all simulations with one exception in Figure 15, where we seed 10,000 particles in a $2° \times 2°$ area to study the transport effect instead of just stirring geometry.

b. Numerical experiments and results. As mentioned in the introduction, wave motions in the mid-depth equatorial Atlantic are most likely driven indirectly by the seasonal variation of the surface wind-stress and the tropical instability wave generated by the strong shear between SEC and NECC. In this scenario, variability in the deep oceans is generated through vertical propagation of wave energy. However, it is also possible that wave-like motions in the interior of the equatorial Atlantic are generated by scattering of a coastally-trapped wave near the equator or by flow interacting with bottom topography. Though the generation mechanisms for wave motions in the deep equatorial Atlantic are not entirely clear at this moment, it is not the purpose of this study to address this issue. Our focus is on stirring and transport induced by wave motions, rather than on the generation of these waves. With this goal in mind, we conducted three sets of numerical experiments, each of which is carefully designed to emphasize the effects of the annual long Rossby wave, the high-frequency Yanai wave, and the combination of these waves on stirring and transport of equatorial water particles. In the following, we describe the forcing configuration and results of each experiment in detail.

In the first set of experiments, we mimic the effects of long annual Rossby waves by forcing the model ocean with a patch of symmetric forcing in the continuity equation. A similar forcing configuration was used by Thompson and Kawase (1993). The forcing is located close to the eastern boundary and its period is one year ($T = 365.25$

days). To minimize the effects of other equatorial waves, the structure of the forcing is that of a first-meridional-mode Rossby wave, that is

$$Q_1(x, y, t) = C_0(q(y) + r(y)) \exp(-((x - 30°)/C_1)^2) \sin(2\pi t T^{-1} + \phi) \quad (18)$$

where $q(y), r(y)$ are defined as in (9) and (10); $\phi = 0$; $C_0 = 1.875 \times 10^{-8}$ cm s^{-1} and $C_1 = 1.25°$ are two constants which determine the strength and zonal e-folding scale of the forcing. The values of C_0 and C_1 are chosen to keep the maximum zonal speed for the excited long Rossby wave in the interior reach about 12 cm s^{-1} (not to exceed 15 cm s^{-1}), because a similar zonal-oscillating speed (10 − 15 cm s^{-1}) in the interior equator was observed in Richardson and Schmitz (1993), Weisberg *et al.* (1979) and Weisberg and Morgan (1981). Before Lagrangian particles are deployed, the model is spun up for two years with the idealized annual forcing. An equilibrium response results in the interior after the annual Rossby wave and Kelvin wave have propagated across the basin. Along the western boundary, on the other hand, flow continues to evolve as short Rossby waves are generated by reflection of the long Rossby wave (Cane and Sarachik, 1981; Gent, 1981).

After the model ocean is spun up, the ensemble of 40,000 particles is released and tracked for two years. Before proceeding to discuss the chaotic stirring induced by the waves, it is useful to examine the residual circulations produced by nonlinearity in the model. Since the flow field is dominated by wave motions, one anticipates that the Eulerian and Lagrangian residual velocity fields will be quite different. The Eulerian residual velocity field is easily obtained by time-averaging the modeled velocity at each grid point over the forcing period T:

$$\bar{\mathbf{u}}_E = \frac{1}{T}\int_0^T \mathbf{u}(t)\, dt \quad (19)$$

Another useful Eulerian quantity which gives an estimate of the vertically-integrated mass transport is the residual transport velocity:

$$\bar{\mathbf{u}}_T = \frac{\int_0^T \mathbf{u}(t)[H + \eta(t)]\, dt}{\int_0^T [H + \eta(t)]\, dt} \quad (20)$$

where H and $\eta(t)$ are the mean and perturbed depths of the water column. The Lagrangian residual velocity is:

$$\bar{\mathbf{u}}_L = \frac{\mathbf{X}(T) - \mathbf{X}(0)}{T} \quad (21)$$

where $\mathbf{X}$ (0) and $\mathbf{X}$ (T) are the positions of the particles at the onset of the integration and after one forcing period, respectively.

Figure 9 shows these three velocities (19)–(21) in an equatorial region of the

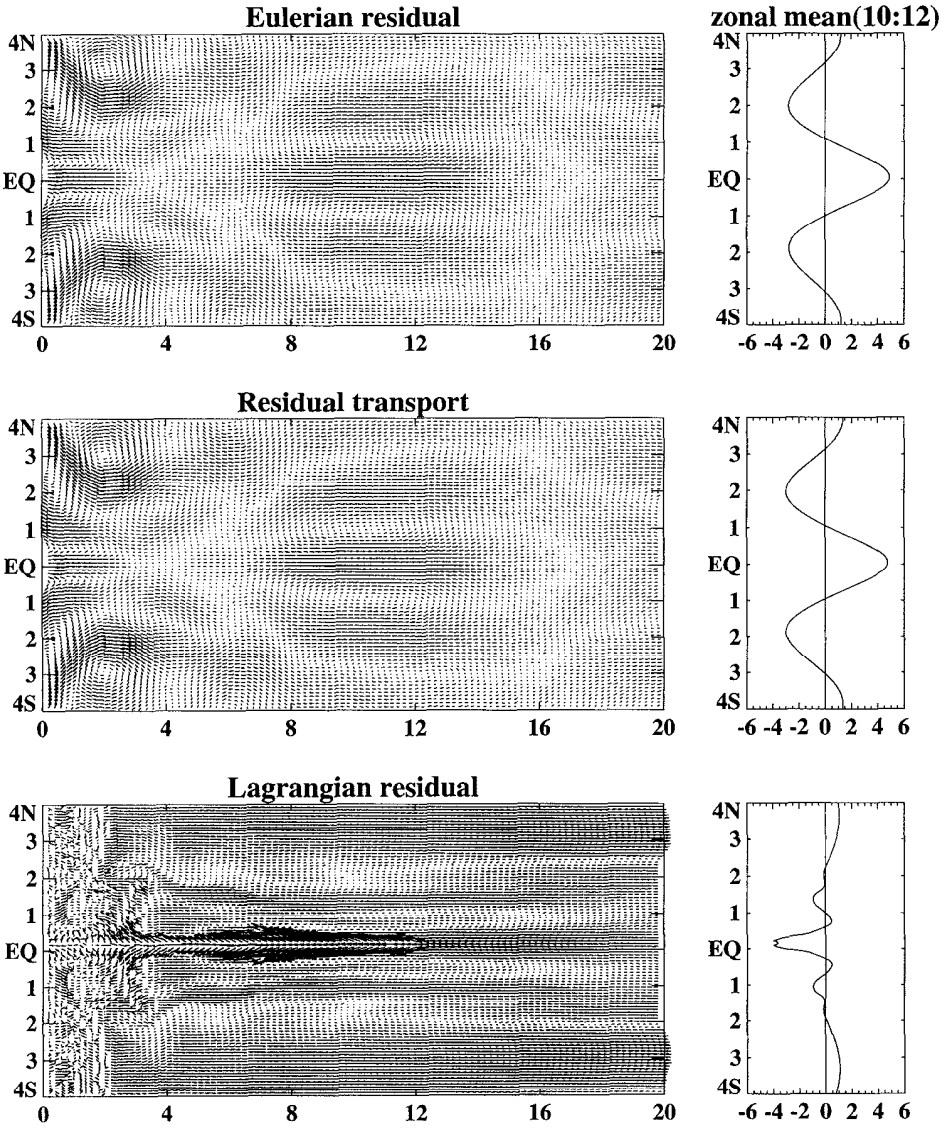

Figure 9. Residual velocities from nonlinear model (a) Eulerian residual velocity ($\bar{\mathbf{u}}_E$); (b) Residual transport velocity ($\bar{\mathbf{u}}_T$); (c) Lagrangian residual velocity ($\bar{\mathbf{u}}_L$). The left panels are velocity vectors. The right panels are zonally-averaged of the above three residual velocities (zonal component) between 10° and 12° (unit: cm s^{-1}), respectively.

model domain. Both the Eulerian residual velocity and the residual transport velocity show intensified flows near the equator and along the western boundary, indicating relatively strong nonlinear effects in these regions. Of particular interest is the eastward Eulerian current in the interior equatorial region, which flows in the

opposite direction to the Lagrangian velocity (Fig. 9c). This result demonstrates that water-particle spreading cannot be computed simply from the Eulerian velocity field.

To gain further insights into the relation between Eulerian and Lagrangian circulations, we conducted a similar numerical experiment with a linear model that has exactly the same parameters. Figure 10 shows three residual velocities from the linear model integration. As expected, both Eulerian velocities shown in Figure 10(a) and (b) are negligibly small. However, the Lagrangian residual velocity ($\overline{\mathbf{u}}_L$) is stronger (Fig. 10c) than that in the nonlinear case (Fig. 9c), indicating that part of the Lagrangian flow was cancelled by the Eulerian flow in the nonlinear model. This result is consistent with Moore's (1970) theoretical prediction that the Stokes' drift is weakened when nonlinear dynamical effects are taken into consideration. Furthermore, in a linear model, the zonally-averaged Lagrangian circulation is essentially the same as the Stokes' drift. In our case, since the long annual Rossby wave dominates the flow field, the zonally-averaged Lagrangian velocity shown in Figure 10(c) agrees well with the Stokes' drift of the long Rossby wave as shown in Figure 2(d).

Stirring induced by the wave motions is expressed in terms of finite-time estimates of Lyapunov exponents. Figure 11a shows the spatial distribution of finite-time Lyapunov exponents at the end of a half year. Recall that strong chaotic stirring is characterized by large positive values of Lyapunov exponents, whereas zero or negative values of the Lyapunov exponents indicate the absence of chaotic stirring. From Figure 11a, the western boundary is a region of strong chaotic stirring. The combined effects of short and long Rossby waves likely contribute to the chaotic stirring of water particles in that region. However, nonlinear wave-wave interaction can occur at western boundary. Therefore, stirring in this region can be more complicated than the one indicated by chaotic stirring theory. Along the equator, chaotic stirring is also strong, particularly in the west. However, the value of Lyapunov exponent attenuates rapidly toward the interior, indicating a rapid decrease in stirring. The reduced chaotic stirring in the interior equator arises because short Rossby waves, which play a major role of stirring fluid, cannot propagate far into the interior from the western boundary before being damped by dissipation. Should there be other equatorial waves which could propagate into the interior, such as the Yanai wave, the zone of strong chaotic stirring would reach far into the interior equatorial ocean, as demonstrated in later experiments.

To reaffirm that chaotic stirring essentially results from linear wave motions, we compare the finite-time estimates of Lyapunov exponents derived from the nonlinear model (Fig. 11a) with those from the linear model (Fig. 11b). Despite differences in detailed structure (particularly along the western boundary), the macrostructure of the Lyapunov exponent distributions is fundamentally the same in both cases; that is, the western boundary and equatorial waveguide are regions of strong chaotic stirring. This result suggests that the nonlinear dynamical effects are not essential in determining the large-scale pattern of wave-induced stirring. They do, however,

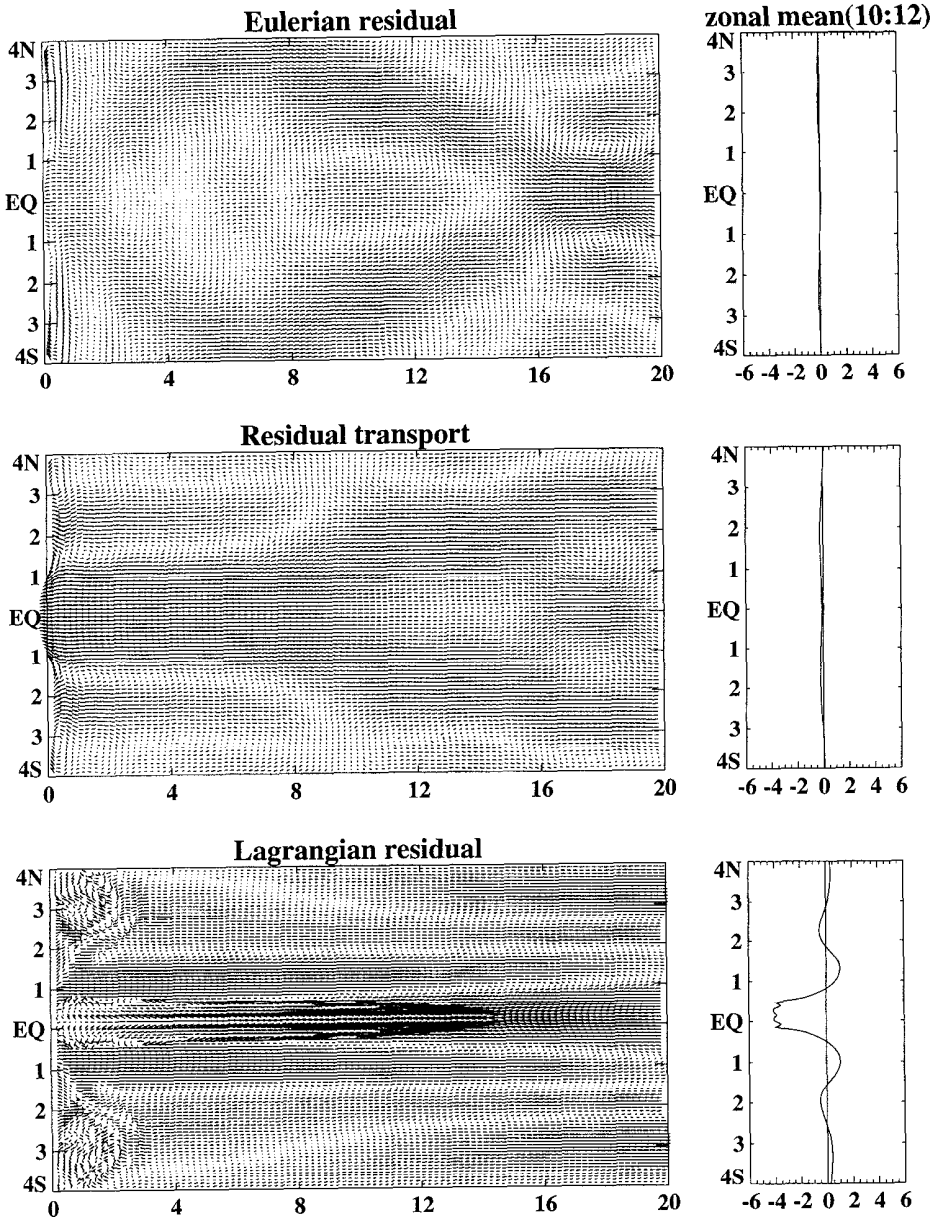

Figure 10. As Figure 9 but from linear model.

affect the detailed stirring processes in regions where nonlinearity is strong, such as the western boundary.

In the second set of experiments, the model ocean is driven by an oscillating force with a period of 45 days in the continuity equation located at the northwestern corner

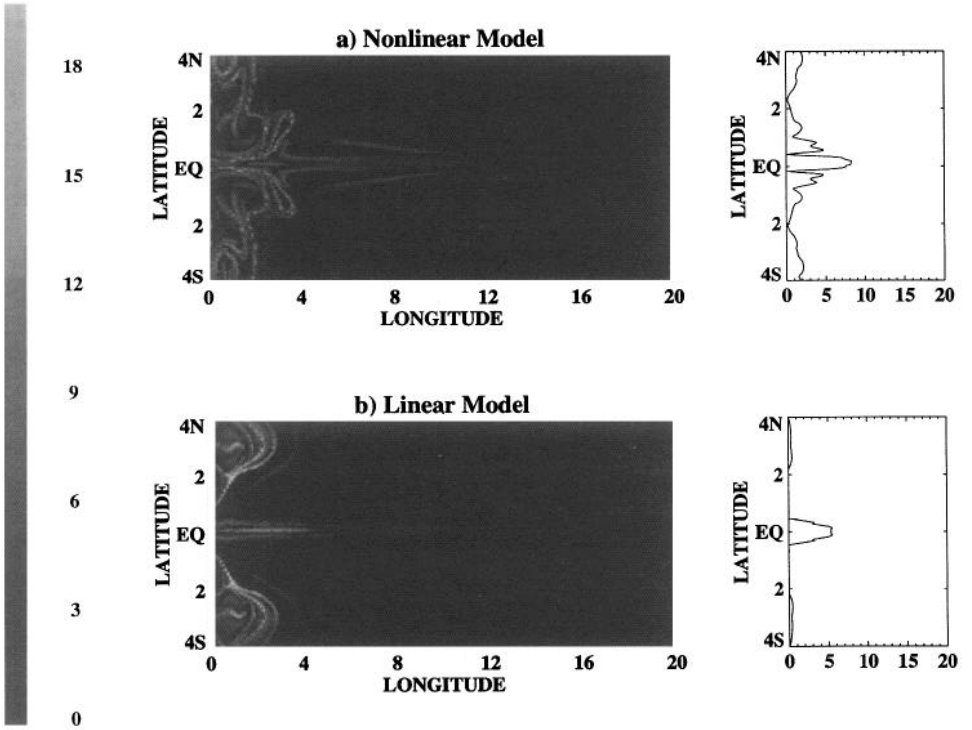

Figure 11. Maps of finite-time Lyapunov exponents (λ) plotted according to starting position of the trajectory at 0.5 year [(a) from nonlinear model; (b) from linear model]. The right panels are zonally averaged between 5° and 10°. The unit is 10^{-8} sec^{-1}.

of the model domain. The precise form of the forcing function is given by

$$Q_2(x, y, t) = C_0\left[\tanh\left(\frac{y - y_0}{2^\circ}\right) - \tanh\left(\frac{y - y_1}{2^\circ}\right)\right]\exp\left(-\frac{x}{C_1}\right)\sin\left(2\pi t T^{-1}\right) \quad (22)$$

where we chose $y_0 = 10.5°, y_1 = 14.5°, C_0 = 1.447 \times 10^{-5}$ cm s^{-1} and $C_1 = 1.45°$. This particular form of forcing is chosen to excite the high-frequency Yanai wave in the interior equatorial ocean through scattering of coastally-trapped Kelvin waves near the equator. The values of C_0 and C_1 are chosen to keep the maximum meridional oscillating speed in the interior reach to 10 cm s^{-1} (not exceed 15 cm s^{-1}) because a similar scale of meridional oscillation was observed in Weisberg *et al.* (1979) and Weisberg and Norigan (1981). Admittedly, such forcing may be artificial given that the high-frequency Yanai waves in the deep equatorial ocean are most likely to be generated by the vertical propagation of wave energy of the near-surface instability waves as suggested by the OGCM simulations (Böning, 1993; Cox, 1980). However, as mentioned earlier, we are interested in the stirring and transport induced by the wave, rather than the wave source itself. Therefore, the detailed wave generation

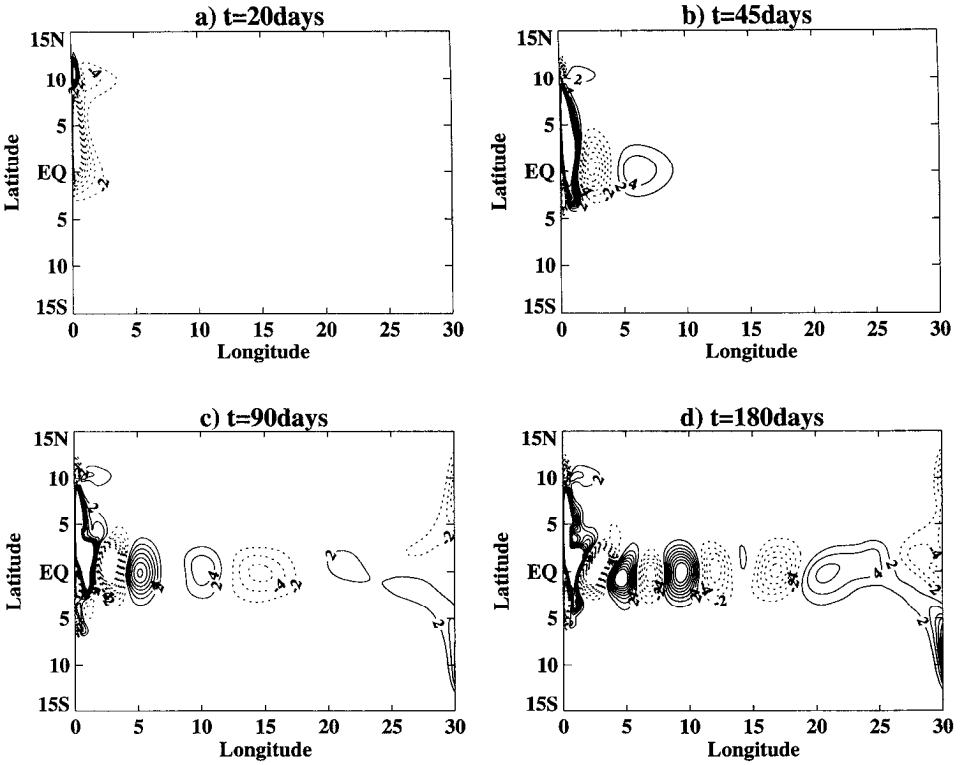

Figure 12. The evolution of flow field (contour of meridional velocity) in NW 45 days forcing case at (a) 20; (b) 45; (c) 90 and (d) 180 days. The interval of contour is 2 cm s^{-1}, with no zero contour.

mechanism does not concern us provided that it generates sufficiently strong wave motions in the interior.

Figure 12 shows the spin-up process of the flow field. It takes the model about 180 days to reach equilibrium. Because the forcing is asymmetric about the equator and, at the given frequency, the only available scattered equatorial waves are the equatorial Kelvin and Yanai waves, there is equipartition of energy between the equatorial Kelvin wave and Yanai wave as the coastal Kelvin wave diffracts at the equator. The equatorial Kelvin wave propagates rapidly eastward along the equator and its energy is ultimately damped by the strong model friction along the northern and southern boundaries. Thus, after reaching equilibrium, the flow in the interior is dominated by the Yanai wave (Fig. 12). Despite the relatively large wave velocity (the maximum instantaneous velocity is on the order of 10 cm s^{-1}), the residual circulation induced by the high-frequency waves is negligibly small (less than 0.5 cm s^{-1}) in the interior (not shown). Stirring is also weak, as indicated by the finite-time Lyapunov exponents (Fig. 13). This result, together with the result in the previous experiment, suggests that a single-frequency traveling wave alone cannot

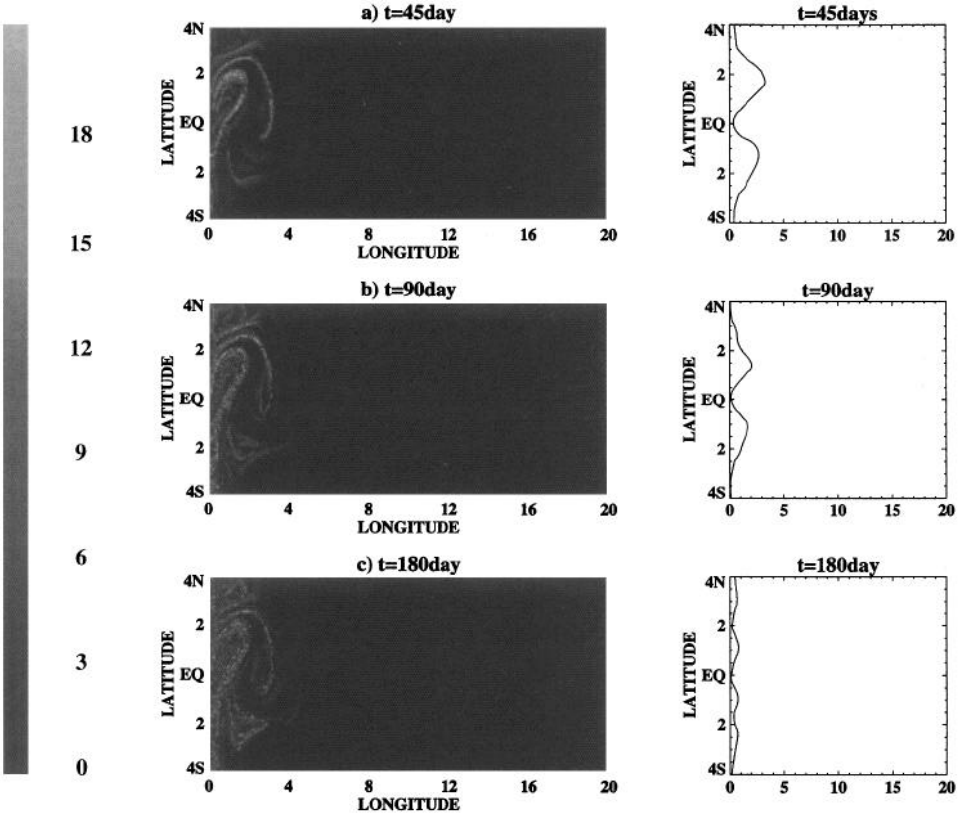

Figure 13. Sequence of maps of finite-time Lyapunov exponents (λ) for NW 45 days forcing case at (a) 45; (b) 90 and (c) 180 days. The right panels are zonally-averaged between 5° and 10°. The unit is same as in Figure 11.

produce chaotic stirring in the interior equatorial ocean. This supports the results of the kinematic stirring analysis.

In the third set of experiments, the model ocean is forced simultaneously by Q_1 and Q_2 at both high- and low-frequencies, so that the interior flows are dominated by both long annual Rossby and 45-day Yanai waves. Time-longitude plots of zonal and meridional components of the equilibrium velocity along the equator indicated that the zonal velocity is dominated by the annual Rossby wave and the meridional velocity by the 45-day Yanai wave (not shown).

To uncover detailed wave-induced stirring processes, Figure 14 depicts the time evolution of the finite-time Lyapunov exponents in the western equatorial region. In contrast to the previous experiments, chaotic stirring along the equator is enhanced significantly. The high-frequency Yanai wave expedites stirring and extends it far into the interior along the equator. Stirring is initially confined near the western boundary owing to the effects of short annual Rossby and high-frequency Yanai

waves. The spatial pattern of the finite-time Lyapunow exponents at this stage (Fig. 14a–c) is similar to that of single Yanai wave case (Fig. 13). At t = 6 months, stirring extends 15° eastward along the equator. In comparison with the case of single Rossby wave (Fig. 11), stirring along the equatorial waveguide is greatly intensified. As time progresses, the finite-time Lyapunov exponents in the interior equatorial region continue to increase. At the end of the two-year simulation, a tongue of high-value Lyapunov exponent emerges along the equator, expanding wider and penetrating farther (reaching 17°) into the interior with an interesting wave patterns (Fig. 14e).

Further details of the stirring and transport are revealed by tracking a cloud of 10,000 particles initially located very close to each other within a 2° × 2° square box centered at (4°, 0°). Figure 15 shows the time-evolution of the particle patch. It is quickly stretched into a nearly-triangular folded filament after one month of integration (Fig. 15a–b). Between one and three months, stretching continues and the filament evolves into a more complicated pattern (Fig. 15c). At t = 5 months (Fig. 15d), it starts to break up into small pieces. After this stage, particles begin to spread randomly near the western equatorial region and gradually move eastward along the equator. Finally, after tracing the particles for two years, an equatorial tongue of more or less uniformly distributed particles forms, indicating a nearly homogenized tracer field. If one follows the eastward movement of the particles closely, the average transport speed is about 1.75 cm s^{-1}.

In the above experiments, the model ocean is forced with oscillatory forcing and thus no permanent DWBC forms. To include the effects of DWBC, an additional experiment is made including a steady high-latitude forcing in the northwestern corner of the model domain. Previous studies by Kawase (1987) and Springer and Kawase (1993) have shown that salient features of the DWBC can be captured by a single-layer, inverted, reduced-gravity model with steady forcing in the continuity equation at high-latitude. Consistent with previous studies (Kawase *et al.* 1992; Springer and Kawase, 1993), our results show little evidence that a steady equatorial current forms when steady forcing is included in the northwestern corner unless unrealistically strong damping is used in the eastern equatorial region. Furthermore, inclusion of steady DWBC appears to have little impact on the stirring properties along the equator in the interior.

We end this section with a few remarks on the consequences of the chaotic stirring on mixing of potential vorticity in the equatorial region. First, due to strong divergence of the equatorial flow, equatorial circulation is not entirely determined by potential vorticity dynamics. In particular, the Yanai wave, which plays a central role in the chaotic stirring, is a mixed vorticity-gravity wave. Therefore, the chaotic stirring induced by this wave will not be manifested as strongly in a potential vorticity field as in a passive tracer field. Numerical experiments indicate that the strength of potential vorticity mixing along the equator depends on both the frequency and

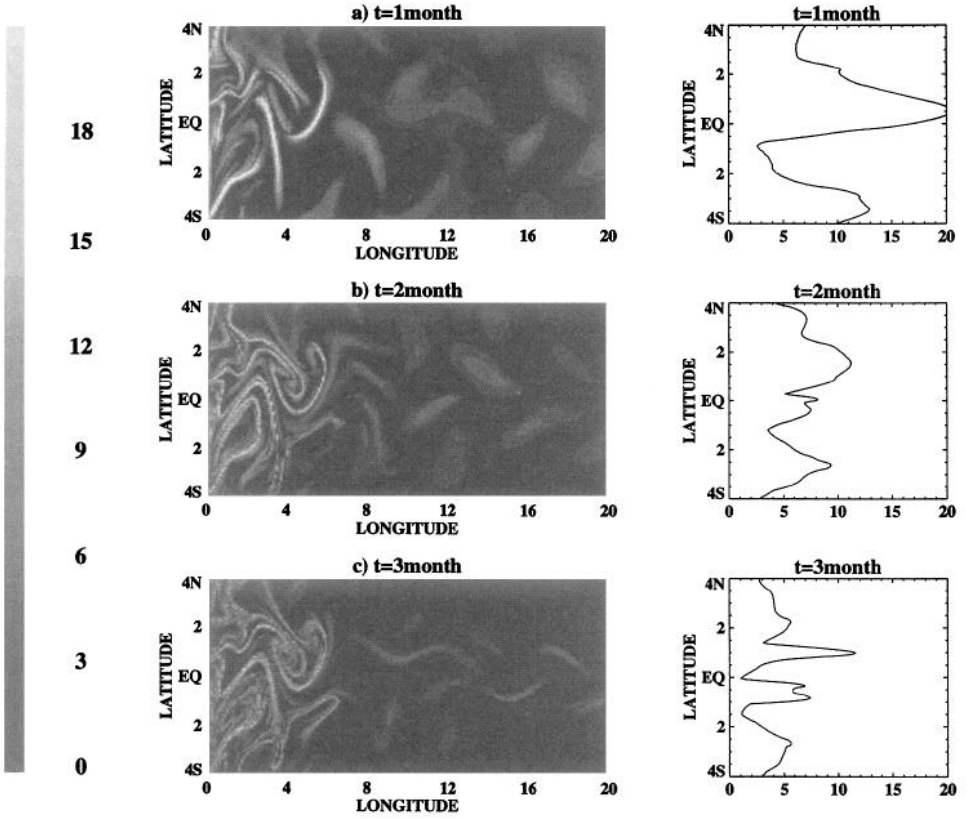

Figure 14. Sequence of maps of finite-time Lyapunov exponents (λ) for both forcings case at 1, 2, 3, 6, 12 and 24 months. The right panels are zonally-averaged between 10° and 15°. The unit is same as in Figure 11.

strength of the Yanai wave, assuming that the annual long Rossby wave is given. The lower the wave frequency and the larger the wave amplitude, the stronger the potential vorticity mixing. This is because the Yanai wave behaves more like a Rossby wave in the low-frequency limit and thus it carries more potential vorticity. Second, potential vorticity is not a passive, but an active tracer. As pointed out by Pierrehumbert (1991a), the key difference between the two is that potential vorticity, owing to its self-induced rotation, can resist being sheared out by a large-scale flow field. Pierrehumbert (1991a) studied chaotic stirring of potential vorticity in great detail in the context of a barotropic vorticity model which contains only vorticity waves; i.e., Rossby waves. He demonstrated that if the large-scale strain provided by the basic flow is sufficiently strong compared to the small-scale potential vorticity, then the latter may be dispersed in a fashion qualitatively similar to the passive tracer dispersion produced by chaotic stirring. In our study, however, since one of the waves (Yanai) involved in the stirring process is not a pure vorticity wave, we observe

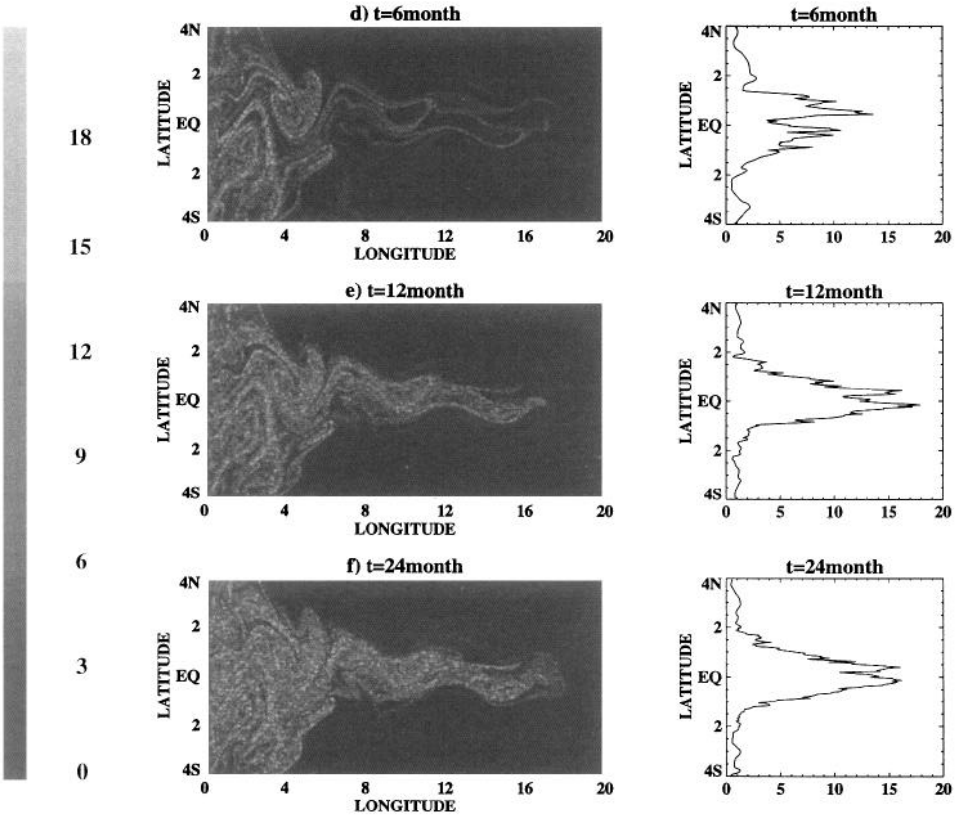

Figure 14. (Continued)

evidences of potential vorticity stirring along the equator only when the frequency of Yanai wave is low (not shown).

4. Conclusions and discussion

A wave-induced stirring and transport mechanism in the mid-depth equatorial ocean is proposed and examined by means of both the analytic linear equatorial wave solutions and a fully nonlinear reduced-gravity model. The study of kinematic stirring using the linear solutions suggests that a superimposition of a few simple equatorial waves can lead to strong Lagrangian stirring and transport along the equator. A combination of an annual long Rossby wave and a high-frequency Yanai wave appears to be most efficient in producing strong stirring in the interior equatorial region. Studies of particle dispersion and stirring rate indicate that the stirring and transport takes the form of "anomalous" diffusion which differs considerably from the turbulent diffusion in the sense that the former requires no random velocity fluctuations in the Eulerian field. This stirring mechanism is proposed as a

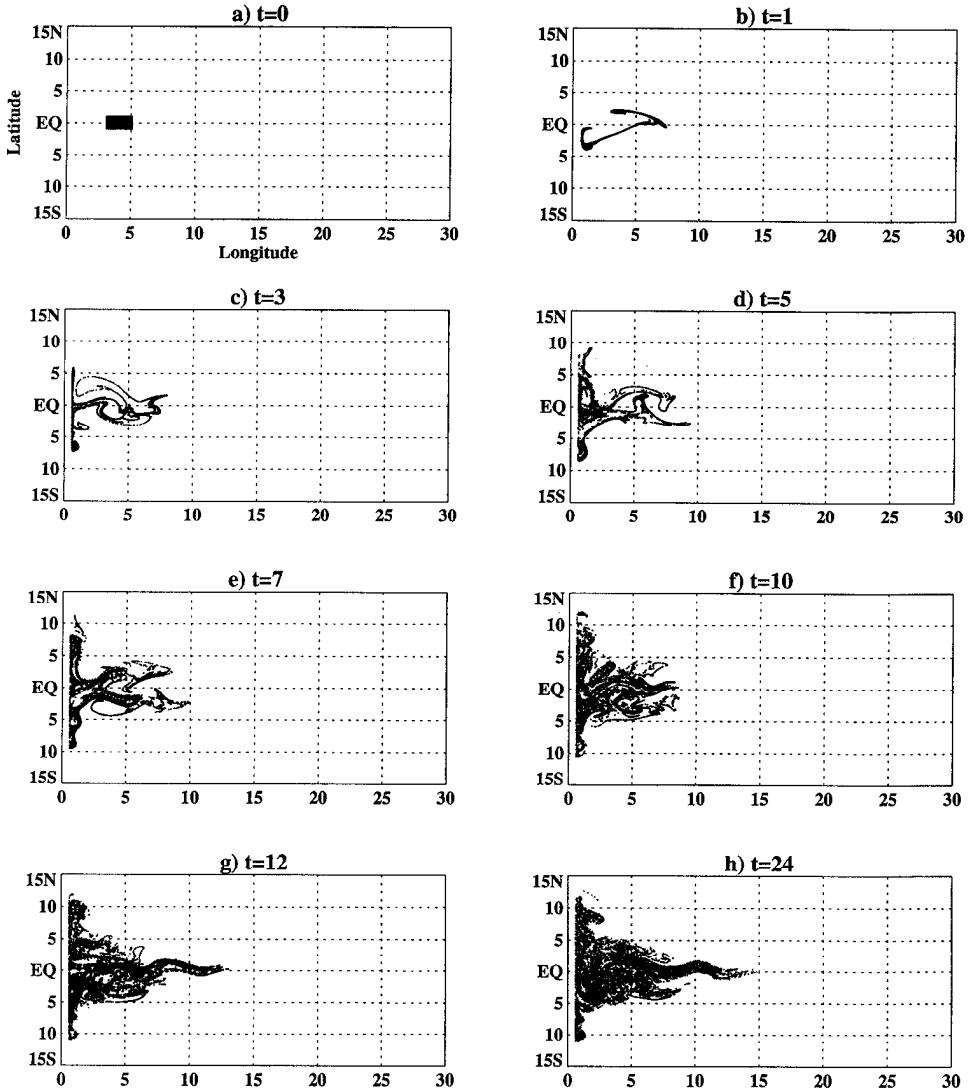

Figure 15. Dispersion of a patch of particles (10,000) for both forcing case at 0, 1, 3, 5, 7, 10, 12, 24 months.

plausible explanation for the observed CFCs tracer field in the mid-depth equatorial Atlantic Ocean (Weiss *et al.,* 1985; Weiss, 1990).

Further investigations of stirring using an inverted, fully nonlinear reduced-gravity shallow-water model support the kinematic stirring study. The comparison between linear and nonlinear model simulations indicates that weakly nonlinear effects of wave dynamics do not have a significant impact on the effective chaotic stirring. By evaluating the finite-time Lyapunov exponents, we identified two regions where

chaotic stirring is most active. One of them is the interior equatorial waveguide where the combination of an annual long Rossby wave and a high-frequency Yanai wave determines the stirring properties. The spatial distribution of the finite-time Lyapunov exponents bears a striking resemblance to the CFCs distribution in the simulations where both a low-frequency Rossby wave and a high-frequency Yanai wave are present in the equatorial ocean interior. The low-frequency Rossby wave prescribes the stirring geometry, whereas the high-frequency Yanai wave plays a role of stirring the fluid. If either wave is absent, stirring cannot extend far into the interior along the equatorial waveguide.

The other strong stirring region is in the vicinity of the western boundary where short Rossby waves likely play a dominant role. In reality, the dynamics of the DWBC and its recirculation are very complicated. Flows in this region are likely to be more turbulent than along the equator. As an example, Thompson and Kawase (1993) found, in their reduced-gravity model simulations, that with only a single-frequency forcing symmetric about the equator at the eastern boundary, the response near the western boundary exhibits strong nonlinear behavior. When the interior flow is eastward, a recirculation gyre sets up, which has dynamics similar to the mid-latitude recirculation of the Gulf Stream. On the other hand, Springer and Kawase (1993) showed that a complicated nonlinear structure of a DWBC can exist even when the reduced-gravity model is forced by a steady mass source near the western boundary corner. Overall, there are many different physical processes (McCartney, 1993) such as formation of coherent nonlinear eddies and nonlinear wave-wave interactions, that contribute to strong stirring of water particles. The SOFAR float trajectories (Richardson and Schmitz, 1993) provide salient evidence of complicated stirring processes in this region.

From the evolution of particle (passive tracer) clouds by means of finite-time estimates of Lyapunov exponents, we have learned that a tracer released within a chaotic zone ultimately becomes uniformly stirred even if a two-dimensional flow is composed of simple wave motions. However, the sequence of events by which the homogenization occurs cannot be described in terms of an eddy diffusivity because the stirring mechanism involved is different from the turbulent diffusivity (Pierrehumbert, 1993). This implies that we must reconsider the problem of stirring parameterizations in situations where wave-like motions dominate the flow field, such as in the deep equatorial oceans, to represent the sub-grid scale process in a noneddy-resolving ocean general circulation model (OGCM). Recent investigation by Pierrehumbert and Yang (1993) and Bowman (1995) suggest that the effectively random phase of wave-breaking events with respect to an individual particle can result in a macroscopic "random walk" of the particle. Under this condition, diffusive models may be a good representation of the ensemble-average transport effects of the flow. However, they do not represent microstructure of the mixing process. Bowman (1995) further proposed a new approach to parameterization of mixing in numerical

models. The required parameters are the distributions of the frequency, width and location of wave-breaking events. A similar approach may be applied in an equatorial ocean to investigate to what extent bulk transport due to wave-induced stirring can be modeled in terms of diffusive models.

This study represents a first attempt to address the role of wave-induced stirring and transport in the mid-depth equatorial oceans. Many of our approximations are likely to oversimplify real oceanic processes. Hence, further investigations are needed to validate the results under more realistic conditions. First of all, the waves in this study are generated by artificial forcings. In reality, waves in the deep oceans are most likely associated with vertical propagation of energy excited by near-surface processes, such as the low-frequency variability of surface winds and the tropical instability waves. Furthermore, the waves propagate through a continuously-stratified ocean where the stratification varies in space and time. Both vertical wave-propagation and stratification effects are ignored in this study. Secondly, the stirring processes presented here are generated by quasi 2-D wave motions, whereas, strong vertical motion in the equatorial oceans could also influence the stirring and transport along the equator. Finally, effects of irregular coastal lines and bottom topography have not been included. It is well-known that the irregular coastal boundary and bottom topography affects the deep circulation through "topographic stirring." However, the extent to which bottom topography influences equatorial flows and associated stirring and transport is not clear. Currently, these issues are being examined in a high-resolution OGCM forced with realistic boundary conditions. The result of this study will be presented in subsequent papers.

Acknowledgments. We thank R. F. Weiss and M. J. Warner for permission to use their unpublished picture of CFCs distribution in 1987–88. The authors would also like to thank R. L. Panetta and K. P. Bowman and three anonymous reviewers for their comments and suggestions during the preparation of this manuscript. This work was supported by National Science Foundation grant OCE-9217036. One of us (P. Chang) is also supported by the NSF Young Investigator Award OCE-9357860.

APPENDIX

Stokes' drift of linear equatorial wave

As a first order approximation in a simple progressive long wave, the difference between the Lagrangian and Eulerian mean velocity accompanying the wave motion is given by the Stokes' drift (Longuet-Higgins, 1969, 1972), i.e.

$$\textbf{Lagrange} = \textbf{Euler} + \textbf{Stokes} \tag{A.1}$$

If the Lagrangian velocity $\mathbf{v}(\alpha, t)$ is defined as

$$\mathbf{v}(\alpha, t) = \mathbf{u}[\mathbf{y}(\alpha, t)] \tag{A.2}$$

where $\mathbf{u}$ is the Eulerian velocity, α is the label of the fluid particle and $\mathbf{y}$ is particle

trajectory given by

$$\mathbf{y}(\alpha, t) = \alpha + \int_0^t \mathbf{v}(\alpha, t')\, dt' \tag{A.3}$$

then it is readily shown that (A.1) can be written in a mathematical form

$$\langle \mathbf{v}(\alpha, t) \rangle = \langle \mathbf{u}(\alpha, t) \rangle + \left\langle \left[\int_0^t \mathbf{v}(\alpha, t')\, dt' \right] \cdot \nabla_\alpha \mathbf{u}(\alpha, t) \right\rangle + \cdots \tag{A.4}$$

where $\langle\ \rangle$ denotes a time average. The second term on the right-hand side of (A.4) is defined as Stokes' drift, which is due to spatial variations of the total Eulerian velocity field.

In the case of free equatorial waves, the Stokes' drift induced by the individual wave component is given by

for Rossby waves: $(n > 1)$

$$U_s = \frac{A_n^2}{2\omega}\left[\frac{k\beta C}{2}\left(\frac{D_{(n+1)}(z)}{Ck - \omega} - \frac{nD_{(n-1)}(z)}{Ck + \omega}\right)^2 - \beta\left(\frac{n+1}{Ck - \omega} + \frac{n}{Ck + \omega}\right)D_n^2(z) + \frac{\beta z}{2} D_n(z)\left(\frac{D_{(n+1)}(z)}{Ck - \omega} + \frac{nD_{(n-1)}(z)}{Ck + \omega}\right)\right] \tag{A.5}$$

for a Yanai wave: $(n = 0)$

$$U_s = \frac{A_0^2}{2C}\left(\frac{k\omega}{2\beta} D_1^2(z) + D_0^2 - \frac{z}{2} D_0(z) D_1(z)\right) \tag{A.6}$$

for a Kelvin wave: $(n = -1)$

$$U_s = \frac{A_0^2}{2C} D_0^2(z) \tag{A.7}$$

where ω is the wave frequency, k is the wave number, C is the phase speed of the equatorial Kelvin wave, A_n is the wave amplitude, $D_n(z)$ is the parabolic cylinder function and z is the latitude nondimensionalized by the equatorial Rossby deformation radius $\lambda = \sqrt{C/(2\beta)}$. A graphic representation of these analytical solutions is given in Figure 2 for an annual Kelvin wave, annual Rossby waves and a 45-day Yanai wave.

Calculation of Lyapunov exponents

Following Pierrehumbert (1991b, 1993), the evolution of a disk of tracer with initially small radius ϵ is considered to define the Lyapunov exponents for the Lagrangian trajectories in a two-dimensional fluid. After a certain time T_0, the disk will have been elongated into an ellipse with axes $a(T_0)$ and $b(T_0)$. If the Lagrangian trajectory is chaotic, at least one of the axes (say, $a(T_0)$) will grow exponentially with time on the average. The elongation rate $\lambda = \log(a/\epsilon)/T_0$ is then defined as the

desired finite-time Lyapunov exponent. In order to compute the Lyapunov exponents, the Euler-Lagrangian transformation Eq. (1) is linearized about some particular trajectory $[X(t), Y(t)]$, writing $x = X + x', y = Y + y'$. The deviations from the trajectory are then governed by

$$\frac{d}{dt}\begin{bmatrix} x' \\ y' \end{bmatrix} = S(t)\begin{bmatrix} x' \\ y' \end{bmatrix}, \tag{A.8}$$

where $S(t)$ is the matrix

$$\begin{bmatrix} \partial_x u & \partial_y u \\ \partial_x v & \partial_y v \end{bmatrix} \tag{A.9}$$

evaluated at the point $[X(t), Y(t)]$. Next, one forms the matrix $M(t)$ satisfying $dM/dt = S(t)M$ subject to the initial condition $M(0) = I$ (the identity matrix). The desired Lyapunov exponent is then given by $\lambda = \log(|\theta|)/T_0$, where θ is the eigenvalue of M with largest modulus.

For a given starting time and time interval T_0, the exponent λ is a function of the position $[x(0), y(0)]$ from which the Lagrangian trajectory is started. By choosing a grid of initial conditions covering some region of interest in the studied domain, the function $\lambda(x, y, T_0)$ can be computed to identify stirring regions. Chaotic stirring is represented by contiguous areas of large λ, while regions of no stirring are indicated by small or vanishing λ.

REFERENCES

Arakawa, A. and V. Lamb. 1981. A potential enstrophy and energy conserving scheme for the shallow water equations. Mon. Wea. Rev, *109,* 18–36.

Aref, H. 1984. Stirring by chaotic advection. J. Fluid Mech., *143,* 1–21.

Böning, K. W. 1991. Deep Equatorial Currents in an eddy-resolving model of the Atlantic Ocean. Abstracts of XX General Assembly of the IUGG. 49 pp.

—— 1993. Deep currents and the eastward salinity tongue in the equatorial Atlantic: Results from an eddy-resolving, primitive equation model, J. Geophys. Res., *98*(C4), 6,991–6,999.

Bowman, K. P.. 1993a. Large-scale isentropic stirring properties of the Antarctic polar vortex from analyzed winds. J. Geophys. Res., *98,* 23,013–23,027.

—— 1993b. Barotropic simulation of large-scale stirring in the Antarctic polar vortex. J. Atmos. Sci., *50,* 2901–2914.

—— 1995. Diffusive transport by breaking waves. J. Atmos. Sci., *52,* 2416–2427.

Cane, M. A. and E. S. Sarachik. 1981. The response of a linear baroclinic equatorial ocean to period forcing. J. Mar. Res., *39,* 651–693.

Cox, M. D. 1980. Generation and propagation of 30-day waves in a numerical model of the Pacific. J. Phys. Oceangr., *10,* 1,168–1,186.

Gent, P. R. 1981. Forced standing equatorial ocean wave modes. J. Mar. Res., *39,* 695–709.

Kawase, M. 1987. Establishment of deep ocean circulation driven by deep-water production. J. Phys. Oceanogr., *17,* 2294–2317.

Kawase, M., L. M. Rothstein and S. R. Springer. 1992. Encounter of a deep western boundary current with the equator: a numerical spin-up experiment, J. Geophys. Res., *97,* 5447–5463.

Kawase, M., and J. L. Sarmiento. 19986. Circulation and nutrients in mid-depth Atlantic waters. J. Geophys. Res., *91,* 9749–9770.

Kessler, W. S. and J. P. McCreary, 1998. The annual wind-driven Rossby wave in the subthermocline equatorial Pacific. J. Phys. Oceanogr., *23,* 1192–1207.

Longuet-Higgins, M. S. 1969. On the transport of mass by time-varying ocean currents. Deep-Sea Res., *16,* 431–447.

—— 1972. On the interpretation of records of time-varing currents. Rapports et Proces-Verbaux des Reunions. Conseil permanent international pour l'exploration de la mer, *162,* 35–41.

Lukas, R. and E. Firing. 1985. The annual Rossby wave in the central Pacific Ocean. J. Phys. Oceanogr., *15,* 55–67.

Moore, D. W. 1970. The mass transport velocity induced by free oscillations at a single frequency. Geophys. Fluid Dyn., *1,* 237–247.

Moore, D. W. and S. G. H. Philander. 1977. Modelling of the tropical oceanic circulation, *in* The Sea, E. D. Goldberg, I. N. McCave, J. J. O'Brien, and J. H. Steele, eds., *6,* Wiley (Interscience), New York. 319–361.

McCartney, M. S. 1993. Crossing of the equator by the deep western boundary current in the western Atlantic Ocean. J. Phys. Oceanogr., *9,* 1,953–1,974.

Ottino, J. M., C. W. Leong, H. Rising and P. D. Swanson. 1988. Morphological structures produced by stirring in chaotic flows. Nature, *333,*419–425.

Philander, S. G. H. 1978. Forced oceanic waves. Rev. Geophys. Space Phys., *16,* 15–46.

Pierrehumbert, R. T. 1991a. Chaotic stirring of tracer and vorticity by modulated traveling Rossby waves. Geophys. Astrophys. Fluid Dyn., *58,* 285–319.

——. 1991b. Large-scale horizontal stirring in planetary atmospheres. Phys. Fluids, *3A,* 1250–1260.

Pierrehumbert, R. T. and H. Yang. 1993. Global chaotic stirring in isentropic surfaces. J. Atmos. Sci., *15,* 2,462–2,480.

Ponte, R. M., J. Luyten and P. L. Richardson. 1990. Equatorial deep jets in the Atlantic Ocean. Deep-Sea Res., *37,* 711–713.

Reid, J. L. 1982. On the mid-depth circulation of the world ocean, *in* Evolution of Physical Ocean, MIT Press, Cambridge, MA, 623 pp.

Richardson, P. L. and W. J. Schmitz, Jr. 1993. Deep cross-equatorial flow in the Atlantic measured with SOFAR float. J. Geophys. Res., *98*(C5), 8371–8378.

Ridderinkhof, H. and J. T. F. Zimmerman. 1990. Mixing processes in a numerical model of the westen Dutch Wadden Sea, residual currents and long-term transport, R. T. Cheng, ed., 194–209.

Sadourny, R. 1975. Compressible model flows on the sphere. J. Atmos. Sci., *32,* 2103–2110.

Semtner, A. J. and R. M. Chervin. 1992. Ocean general circulation from a global eddy-resolving model. J. Geophys. Res., *97*(C4), 5493–5550.

Solomon, T. H., E. R. Weeks and H. L. Swinney. 1994. Chaotic advection in a two-dimension flow: Levy flights and anomalous diffusion. Physica D, *76,* 70–84.

Springer, S. R. and M. Kawase. 1993. Nonlinear and dissipative dynamics in the connection region between western boundary currents and equatorial currents. J. Geophys. Res., *98*(C5), 12,511–12,525.

Stommel, H. and A. B. Arons. 1960a. On the abyssal circulation of the world ocean I. Stationary planetary flow patterns on a sphere. Deep-Sea Res., *6,* 140–154.

—— 1960b. On the abyssal circulation of the world ocean II. An idealized model of the circulation pattern and amplitude in oceanic basins. Deep Sea Res., *6,* 217–233.

Thompson, L. and M. Kawase. 1993. The nonlinear response of an equatorial ocean to oscillating forcing. J. Mar. Res., *51,* 467–496.

Weeks, E. R., T. H. Solomon, J. S. Urbach and H. L. Swinney. 1994. Observations of anomalous diffusion and Levy flights, *in* Levy Flights and Related Topics in Physics, Proc. Intl. Workshop, Nice, France, M. F. Shlesinger and G. M. Zaslavsky, eds., Springer-Verlag, 347 pp.

Weisberg, R. H. and A. M. Horigan. 1981. Low-frequency variability in the equatorial Atlantic. J. Phys. Oceanogr., *11,* 913–920.

Weisberg, R. H., A. M. Horigan and C. Colin. 1979. Equatorially trapped Rossby-gravity wave propagation in the Gulf of Guinea. J. Mar. Res., *37,* 67–86.

Weiss, J. B. 1991. Transport and stirring in traveling waves, Phys. Fluids A, *3,* 1379–1384.

Weiss R. F. 1990. Deep equatorial Atlantic chlorofluorocarbon distributions. EOS, *70,* (Abstract), 1132.

Weis, R. F., J. L. Bullister, R. H. Gammon and M. J. Warner. 1985. Atmospheric chlorofluoromethanes in the deep equatorial Atlantic. Nature, *314,* 608–610.

Wüst, G. 1935. Schichtung und Zirkulation des Atlantischen Ozeans: Die Stratosphäre, Wiss. Ergeb. Dtsch. Atlant. Exp. Meteor. 1925–1927, *6,* 180 pp.

Young, W. R., P. B. Rhines and C. J. R. Garrett. 1982. Shear flow dispersion, internal waves and horizontal stirring in the ocean. J. Phys. Oceanogr., *12,* 515–527.

Zimmerman, J. T. F. 1979. On the Euler-Lagrangian transformation and the Stokes' drift in the presence of oscillatory and residual currents. Deep-Sea Res., *26,* 505–520.

—— 1986. The tidal whirlpool: A review of horizontal dispersion by tidal and residual currents. Neth. J. Sea Res., *20,* 133–154.

Received: *16 May, 1995;* revised: *14 December, 1995.*